SANDIA REPORT
SAND2008-4992
Unlimited Release
Printed August 2008

West Pearl Queen CO_2 Sequestration Pilot Test and Modeling Project 2006-2008

Scott P. Cooper, Lewis C. Bartel, John C. Lorenz, David F. Aldridge, Bruce P. Engler, Neill P. Symons, Charles Byrer, Andrea McNemar, Gregory J. Elbring

Prepared by
Sandia National Laboratories
Albuquerque, New Mexico 87185 and Livermore, California 94550

Sandia is a multiprogram laboratory operated by Sandia Corporation,
a Lockheed Martin Company, for the United States Department of Energy's
National Nuclear Security Administration under Contract DE-AC04-94AL85000.

Issued by Sandia National Laboratories, operated for the United States Department of Energy by Sandia Corporation.

Available to DOE and DOE contractors from
U.S. Department of Energy
Office of Scientific and Technical Information
P.O. Box 62
Oak Ridge, TN 37831

Telephone: (865) 576-8401
Facsimile: (865) 576-5728
E-Mail: reports@adonis.osti.gov
Online ordering: http://www.osti.gov/bridge

Available to the public from
U.S. Department of Commerce
National Technical Information Service
5285 Port Royal Rd.
Springfield, VA 22161

Telephone: (800) 553-6847
Facsimile: (703) 605-6900
E-Mail: orders@ntis.fedworld.gov
Online order: http://www.ntis.gov/help/ordermethods.asp?loc=7-4-0#online

SAND2008-4992
Unlimited Release
Printed August 2008

West Pearl Queen CO_2 Sequestration Pilot Test and Modeling Project 2006-2008

Scott P. Cooper, Lewis C. Bartel, John C. Lorenz, David F. Aldridge, Bruce P. Engler, Neill P. Symons, Charles Byrer, Andrea McNemar, Gregory J. Elbring

Geoscience and Environment Center
Sandia National Laboratories
P.O. Box 5800
Albuquerque, New Mexico 87185

Charles Byrer, Andrea McNemar
Fuel Resources Division
National Energy Laboratory
Morgantown, WV 26507

ABSTRACT

The West Pearl Queen is a depleted oil reservoir that has produced approximately 250,000 bbl of oil since 1984. Production had slowed prior to CO_2 injection, but no previous secondary or tertiary recovery methods had been applied. The initial project involved reservoir characterization and field response to injection of CO_2; the field experiment consisted of injection, soak, and venting. For fifty days (December 20, 2002, to February 11, 2003) 2090 tons of CO_2 were injected into the Shattuck Sandstone Member of the Queen Formation at the West Pearl Queen site. This technical report highlights the test results of the numerous research participants and technical areas from 2006-2008. This work included determination of lateral extents of the permeability units using outcrop observations, core results, and well logs. Pre- and post-injection 3D seismic data were acquired. To aid in interpreting seismic data, we performed numerical simulations of the effects of CO_2 replacement of brine where the reservoir model was based upon correlation lengths established by the permeability studies. These numerical simulations are not intended to replicate field data, but to provide insight of the effects of CO_2.

ACKNOWLEDGMENTS

This work is sponsored by the U.S. Department of Energy, Office of Fossil Energy, with thanks to Charles Byrer and Andrea McNemar, contract managers for this project. The authors also thank Kinder Morgan for donating the CO_2 used for injection during the field test. The authors also gratefully acknowledge their home organizations and each other for their collaboration and support of this research (Sandia National Laboratories, and the National Energy Technology Laboratory). The authors would also like to thank the following individual participants who have helped throughout the life of this project: Rajesh Pawar, Robert Benson, Reid Grigg, James Krumhansl, Norman Warpinski, Carlos F. Jove-Colón, and Bruce Stubbs.

CONTENTS

FIGURES

TABLES

NOMENCLATURE

dB	decibel
DOE	Department of Energy
RTM	Reverse-time migration
SNL	Sandia National Laboratories

1. INTRODUCTION

Carbon dioxide (CO_2) sequestration in geological formations is the most direct carbon management strategy for reducing anthropogenic CO_2 emissions into the atmosphere and will likely be needed for continuation of the global fossil-fuel–based economy. Storage of CO_2 into depleted oil reservoirs may prove to be both cost effective and environmentally safe. However, injection of CO_2 into oil reservoirs is a complex issue, spanning a wide range of scientific, technological, economic, safety, and regulatory issues. Detailed studies about the long-term impact of CO_2 on the host reservoir are necessary before this technology can be deployed.

The main objectives of this project was (1) to characterize the oil reservoir and its sequestration capacity; (2) to better understand CO_2 sequestration-related processes; and (3) to predict and monitor the migration and ultimate fate of CO_2 after injection into a depleted sandstone oil reservoir. The project is focused around a field test that involved the injection of approximately 2090 tons of CO_2 into a depleted sandstone reservoir at the West Pearl Queen Field in southeastern New Mexico. Geophysical monitoring surveys, laboratory experiments, geophysical surveys, and numerical simulations were performed in support of the field experiment. Results show that the response of the West Pearl Queen reservoir during the field experiment was significantly different than expected based on the pre-injection characterization data. Thus, the observations and experimental results show that extensive reservoir characterization is necessary to understand and predict the impact of CO_2 injection on storage reservoirs.

1.1. Geology post-test assessment - Lateral extents of permeability units

Outcrop and subsurface data were analyzed post-test to assess the continuity of reservoir sandstones and potential influence on anomalies observed during the CO_2 sequestration phase at the West Pearl Queen Field. Outcrop exposures indicate that the Shattuck Member sandstones of the Queen Fm were deposited in eolian and eolian-influenced shallow lagoons. Although extensive tabular bedding of homogeneous sandstones is observed, heterogeneities such as facies changes, local bedding thickenings, intraclast conglomerates, channels, and thrust faults are also present. These heterogeneities would interrupt uniform injection of CO_2. The sandstone reservoirs at the West Pearl Queen Field also only superficially appear to correlate between wells as uniform, vertically stacked layers of laterally extensive sandstone. The lack of sandstone continuity and intraformational heterogeneities can explain four anomalies that were observed during CO_2 injection. Specifically, these were the 1) higher than expected injection pressures, 2) resultant lower than expected CO_2 injection rates, 3) apparent localization of the injected CO_2 at the base of the injection well, and 4) inordinately long time (3 years) for breakthrough of the CO_2 into the observation well, located only ¼ mile east of the injection well.

Subsurface and outcrop data were analyzed to assess the continuity of reservoir sandstones and potential influence on anomalies observed during the CO_2 sequestration phase at the West Pearl Queen Field.

Outcrop exposures indicate the Shattuck Member sandstones of the Queen Formation where deposited in eolian and eolian-influenced shallow lagoons. Although extensive tabular bedding

of homogeneous sandstones is observed, heterogeneities such as facies changes, local bedding thickenings, intraclast conglomerates, channels, and thrust fault are also present. These heterogeneities would interrupt uniform injection of CO_2. Estimated average lateral extent of reservoir units from the outcrop data are on the order of 1500 ft (457 m) and are compatible with subsurface data indicating only half of the sandstones extend laterally for more than 1500-1700 ft (457-518 m). Sandy zones interpreted from the well logs and core are also more extensive than their individual component beds and fluid communication within and between zones is limited by low-porosity, fine grained and well-cemented interbeds.

1.2 Seismic Modeling

The West Pearl Queen (WPQ) field carbon dioxide (CO_2) sequestration experimental site is located near Hobbs, New Mexico. Baseline seismic reflection data were acquired in late 2002, prior to injecting ~2100 tons of liquefied CO_2 into a porous sandstone formation at ~1370 m depth. A second, post-injection seismic survey was acquired in mid-2003. All field acquisition conditions were nominally the same for both of these three-dimensional (3D) reflection surveys. The objective of this "time-lapse" (or 4D) seismic experiment is to detect and monitor the CO_2 plume at depth. Differences in the recorded seismic traces may be attributed to changing conditions in the sequestration reservoir induced by injection of CO_2. The purpose of the numerical simulations reported here are not to match the field data but determine appropriate analysis techniques to image the plume utilizing 4D seismic surveys. Even though we do not wish to match the field data, we used model parameters suitable for the WPQ site.

In this report we consider two reservoir models, each determined by observed correlation lengths. Here we consider two different realizations of the random distribution of the P-wave speed, V_p and mass density, ρ throughout the reservoir volume. The effects of CO_2 replacement of brine were modeled using Gassmann's (1951) equation. Even though the changes in wave speeds and mass density are small, a careful comparison of pre- and post-injection simulations demonstrates that the CO_2 target can be detected.

2. Lateral Extents of Permeability Units

The West Pearl Queen is a depleted oil reservoir that has produced approximately 250,000 bbl of oil since 1984. Production had slowed prior to CO_2 injection but no previous secondary or tertiary recovery methods had been applied (Pawar, et al., 2006). The initial project involved characterization and field response to injection of CO_2; the field experiment consisted of injection, soak and venting (Pawar, 2006). For 50 days (December 20, 2002 to February 11, 2003) 2090 tons of CO_2 were injected into the Shattuck Sandstone Member of the Queen Formation at the West Pearl Queen site. The injection rate was 40 tons per day; significantly lower than the 100 tons/day expected from preinjection characterization. Early during injection the surface injection pressure reached 1400 psi and thus the calculated bottom-hole constraint of 2900 psi. This pressure was kept constant for the remainder of the experiment. At the end of the injection phase, the injection well was shut-in and the CO_2 soaked for 6 months. Before venting, a post injection 3-D seismic survey was acquired. The injection well was then connected to a separator and allowed to vent. The well flowed freely for 9 days after which it stopped flowing and a pump was installed. After 3 months only 17% of the total injected CO_2 was recovered and 43% recovered after two years. Pre and post-injection production of oil and water proved to be very similar. It was nearly three years before CO_2 was produced in the nearest production well (data in this introduction from Pawar, et al., 2006).

In light of the experimental responses, such as low CO_2 injection rates, higher than expected injection pressures and a lag in inter-well communication, this study was undertaken to further assess the continuity of reservoir sandstones in the West Pearl Queen Field. Both outcrop and subsurface data were utilized. This paper is divided into two sections detailing these two data sets. Ultimately, this work discusses the implications for sequestration of CO_2 at sites with limited reservoir dimensions and internal low-permeability baffles and the potential ways to recognize these heterogeneities through outcrop and subsurface analysis.

This project is a shared effort that includes the following organizations Sandia National Laboratories, Los Alamos National Laboratories, Strata Production Company, the New Mexico Institute of Mining and Technology, and the Colorado School of Mines.

2.1 Outcrop Assessment of the Lateral Extent of Permeability Units within the Shattuck Sandstone

The outcrops described here are located approximately 60 miles (96 km) west of the West Pearl Queen field (Figure 2.1). The outcropping strata are time-equivalent to the subsurface West Pearl Queen reservoirs, and although widely separated, the two suites of strata are located in similar paleogeographic positions a few miles landward of the local Delaware basin shelf margin, and they display similar sedimentary structures. Therefore the depositional environments are probably similar, suggesting that they have similar lateral extents.

(a) 2.1.1 Methods

This study focused on the Queen Sandstone where it crops out in the area of Rocky Arroyo (Figure 2.2), 15-20 miles (24-32 km) northwest of Carlsbad, NM. Although 60 miles (96 km)

distant from the West Pearl Queen Field; these are the closest outcrops of strata that are equivalent to the CO2 injection reservoirs. Measured sections and photo-mosaics were made of the outcrops, and individual sandstone beds were traced laterally. The distances between the lateral terminations of each bed were measured, noting whether each termination was due to a facies change (i.e., the bed ended naturally, pinching out or transitioning to a different, non-reservoir lithology) or whether it was only an apparent bed termination, caused by to erosion or cover by talus and vegetation.

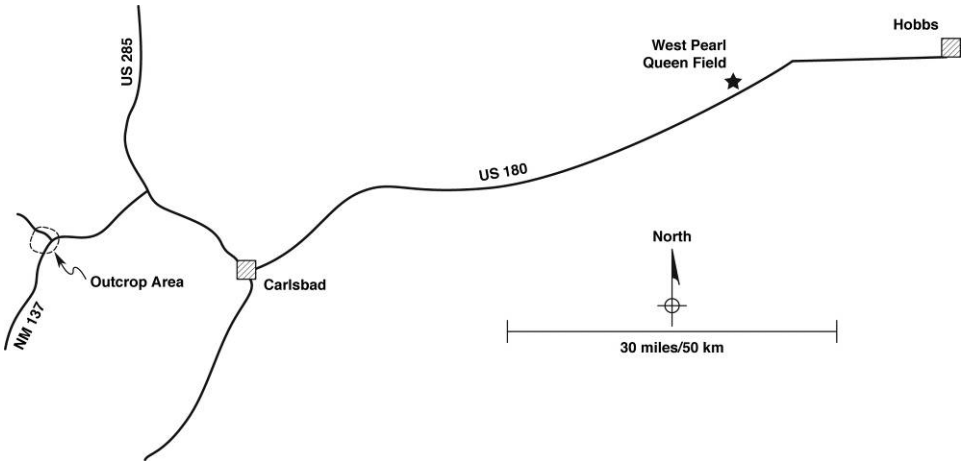

Figure 2.1. Location map of west Pearl Queen field and outcrops investigated for this paper.

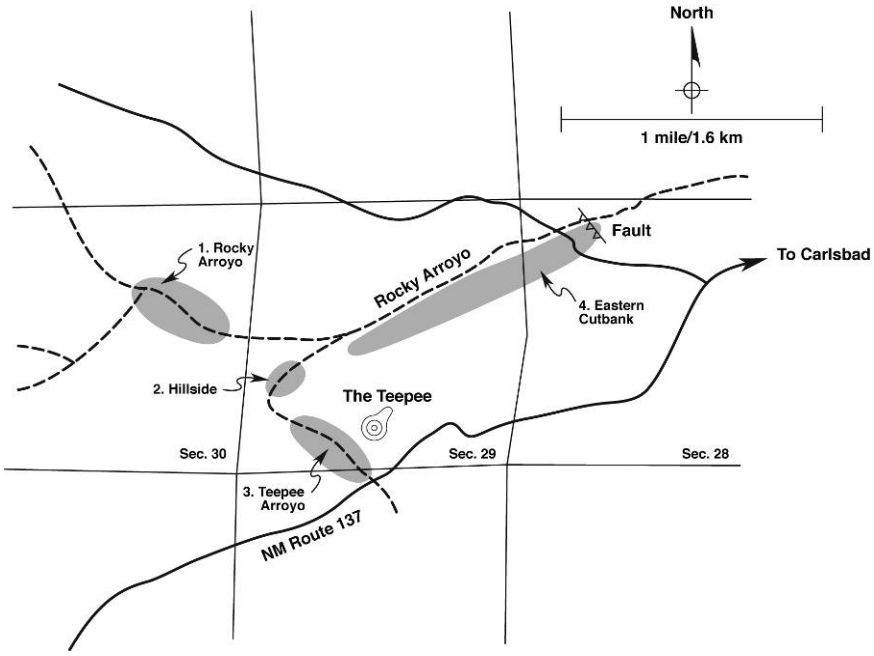

Figure 2.2. Outcrop location map. Discussions in the text will focus on these four primary outcrop locations (Rocky Arroyo, Hillside, Teepee Arroyo, and Eastern Cutbank).

The recessive, weathered/covered nature of the Shattuck sandstones in outcrop presents a problem when trying to measure the lateral extents of individual beds (Figure 2.3). Most of the sandstones of the Shattuck proper are cleanly exposed only in road cuts and a few natural outcrops in arroyo cut banks. These outcrops have lateral dimensions of tens to a few hundreds of feet, and are much smaller than the typical lateral dimensions of reservoir-type sandstones. Because of this, the extents of Shattuck-type sandstones in outcrop can only be measured where they are inter-bedded with thicker dolomites in the upper part of the Queen Dolomite (which underlies the main body of the Shattuck Sandstone). This inter-bedding protects the sandstones from weathering and overgrowth, allowing them to be exposed over longer horizontal distances where conditions are right.

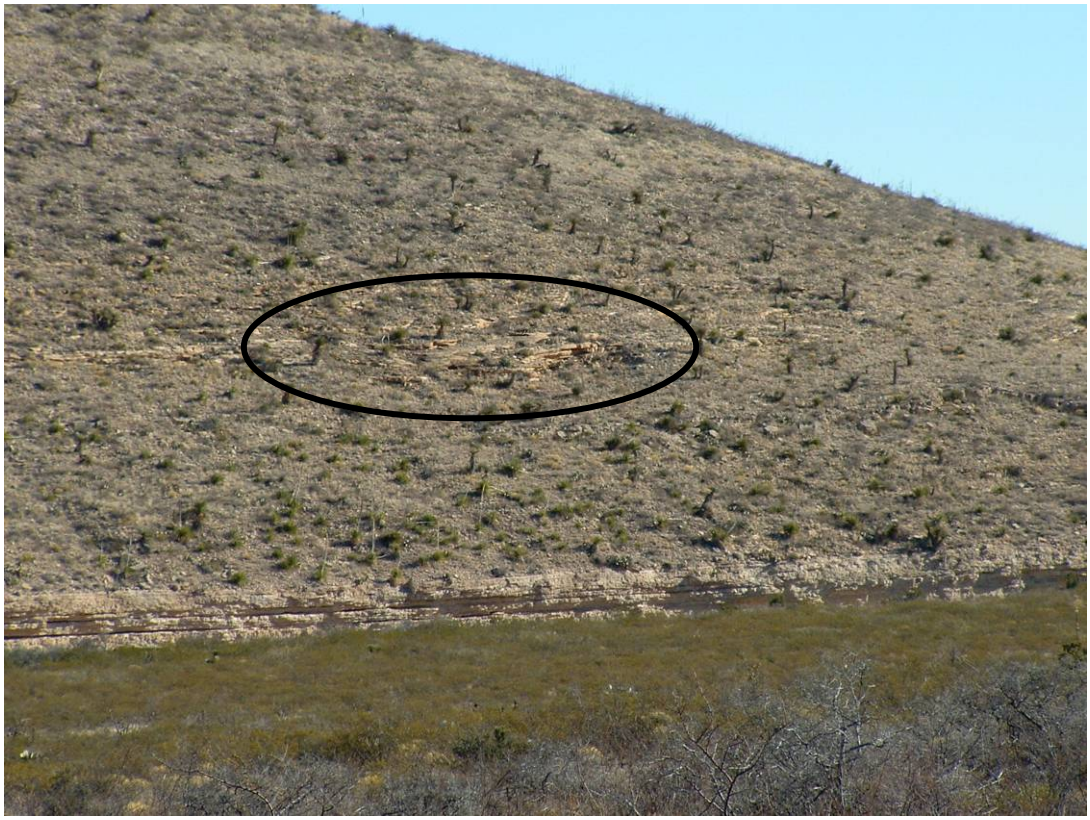

Figure 2.3. Typical "good" natural exposures of the Shattuck Sandstone Member of the Queen Formation, midway up the hill slope. The better outcrops at the base of the hill are of Queen Dolomite in the bottom of Rocky Arroyo.

However, inter-bedding with thick dolomite beds suggests that the depositional environments were not entirely analogous to the dominantly sandy, overlying main body of the Shattuck, and in fact the dimensions measurable in these outcrops suggest more laterally restricted units (see below) than indicated by the earlier subsurface study. Nevertheless, thin dolomite beds are also present throughout the main body of the Shattuck, so the difference is one of degree only.

The Shattuck Sandstone interval in outcrop overlies the Queen Dolomite, and underlies carbonates and evaporates of the Seven Rivers Formation. No easily identifiable, laterally

extensive sandstone, equivalent to the marker bed that was used to bound the upper limit of the zone of interest in the subsurface, could be identified in the poorly exposed outcrops.

2.2 Observations and Interpretations

Sedimentary structures in the Shattuck sandstones that would be diagnostic of depositional environments are poorly defined and difficult to detect because of the uniformly fine-grained nature and mono-mineralic nature of the component sands. Yet enough hints of sedimentary structures are present to suggest that such structures would be common if there were enough heavy minerals or different grain sizes to highlight them. Faint horizontal bedding is the most common feature in the few outcrops where structures are visible (Figure 2.4), and one instance of parting lineation was noted. Examples of ripple marks (Figure 2.5), and small-scale cross bedding (Figure 2.6), are present locally, typically on and near the tops of the beds where they suggest reworking of the deposits in shallow-water environments. Local low-angle bedding (Figure 2.7) and hints of soft-sediment deformation are also present.

Most of these structures suggest deposition in shallow bodies of low-energy water. The one example of parting lineation also suggests shallow, but fast-flowing water. Much of the sand was probably transported to the shallow water environments by winds, some of it as migrating dunes but much of it as dust storms. Low-energy water currents in the lagoons reworked many of the primary eolian deposits, at least their upper parts, into ripples and small cross beds.

Figure 2.4 Obscure low-angle to horizontal bedding, highlighted by erosion.

Figure 2.5 Small, wave-generated ripple marks on the top of a dolomite bed, indicating a shallow water environment.

Figure 2.6. Small cross-beds near the top of a sandstone.

Figure 2.7. Poorly-defined low-angle cross-bedding (below geologist's right knee and at the left side of the picture, suggest low-angle bedding at the toe of a sand dune.

Most of the Shattuck sandstones occur as beds about a half to two meters (1 ½ to 6 ½ feet) thick. Hints of composite bedding (extensive silty and/or more calcareous zones within the thicker sandstones) suggest that the thicker beds are compound units formed by one or more depositional events, similar to the compound reservoir units seen in the subsurface.

One laterally-extensive contact between a sandstone and the underlying dolomite suggests that the sandstone was deposited in a low-energy, shallow-water setting, and that the dolomite comprised an unconsolidated, muddy substrate at the time of sand deposition (Figures 2.7, 2.9). The process that deposited the sand did not rip up the underlying dolomite into an intraclast conglomerate, even though the dolomite mud was soft enough to have oozed into the base of the sand as sand was deposited.

Figure 2.8 Soft-sediment contact between a dolomite and an overlying sandstone (between the two arrows), suggesting that the sand was gently emplaced over a soupy carbonate substrate. The most plausible environment is a shallow lagoon in which carbonate mud was being precipitated. Sand was blown into the lagoon during dust storms, settling gently and vertically through the water to load into the mud (see following figure for close-up of the contact).

Figure 2.9 Close-up of the dolomite and the overlying sandstone from the previous photo, showing the irregular but low-energy nature of the contact.

High-energy conditions such as fluvial flow would have scoured an irregular contact and ripped the carbonate mud up into imbricated intraclasts, whereas this contact suggests vertical loading by gently deposited sandstone.
A plausible depositional scenario for these sandstones is that sand was blown gently but continuously into the shallow lagoons where dolomite mud had been forming. Wind deposition was prevalent in the Permian environments, with dust storm and sand storm deposits being found in both the marine and non-marine settings. Sand dunes were probably common, but were rarely preserved. Some of the Shattuck sandstones may in fact record the basal parts of sand dunes that prograded into shallow lagoons, and the thickness of the sandy beds may record the water depths. One channel form, described below, suggests an interesting dichotomy, wherein some high energy process (possibly a storm) cut a channel into existing sandstones, but later low-energy processes (such as wind-blown sand) filled the channel.

All of the sandstones and dolomites in the outcrops described here are extensively fractured. Natural fractures and their potential effects on reservoir permeability are not the focus of this study, but some of the outcrops display excellent pavements that would lend themselves to a detailed fracture study.

2.3. Local Outcrop Data

(b) 2.3.1. Rocky Arroyo (south half of the northeast quarter, sec. 30, T. 21 S., R. 24 E.)

Six sandstone beds are exposed at this location (see Figure 2.2), inter-bedded within dolomite units of the upper part of the Queen Dolomite in a long cut-bank outcrop on the northern side of Rocky Arroyo as it opens up westward into Indian Basin. The extensive exposure of strata, for about 1500 ft (457 m) along the arroyo, is unique in affording the opportunity to study the dimensions of the sandy units on a scale that is similar to the interwell spacing (500-1900 ft; 152-580 m) at the West Pearl Queen field. The sandstones can be traced laterally because they are inter-bedded with dolomites (Figure 2.10), which protect the softer sandstones from weathering and erosion, and because occasional flooding in the arroyo keeps the face of the outcrop clean. The sandstones are not covered by talus and vegetation at this location as they are in most areas where the main body of the Shattuck sandstone comes to the surface (e.g. Figure 2.3).

The sedimentary structures and scale of bedding in the sandstones are similar to those present in the poorly exposed outcrops above the arroyo where the inter-bedded dolomites are much thinner and do not protect the easily-weathered sandstones. Because the sedimentary structures are similar, we believe that these sandstones represent similar environments, that they have similar lateral extents, and that they can be used for estimating the lateral extents of sandstone reservoir units where they are not inter-bedded with thick dolomites in the overlying Shattuck section and in the equivalent subsurface strata.

Four measured sections and a photo-mosaic show that six sandstone beds, varying from one-half to two-and-a-half meters thick, are present in this outcrop. However, effectively there are seven sandstones and fourteen lateral terminations to assess since one unit grades laterally from sandstone to a sandy dolomite and back again to sandstone in the middle of the outcrop. Six

(43%) of the 14 sand-bed terminations are un-related to depositional changes, being caused by cover and/or erosion, thus some of the measured lateral extents represent only the minimum possible horizontal dimension of the bed. However, the remaining eight known terminations represent a surprisingly large population given the limited extent of the outcrop, and they provide a reasonable basis to begin estimating lateral reservoir dimensions from the outcrop.

Only one of the sandstones can be traced for the entire length of the outcrop, nearly 1400 ft (425 m; Figure 2.11). Its eastern and western ends are covered; therefore 1400 ft (425 m) is a minimum lateral extent. This bed is a composite bed, composed of three sandstone units separated by two thin, silty, recessive units. Small cross beds and ripple marks are present in the upper zones of the lower bed in several of the measured sections, suggesting reworking of the top of that bed in shallow-water conditions. The contact with the underlying dolomite is irregular, suggesting that the carbonate substrate was soft and even soupy at the time of sand deposition. Centimeter-scale iron-oxide (probably iron pyrite before weathering) nodules are present a few tens of centimeters above the basal contact, suggesting an interface between anoxic, organic waters related to the buried algal carbonates, and overlying oxygenated waters.

Figure 2.10. Interbedded sandstones (light orange-brown) and dolomites (light gray) of the upper part of the Queen Dolomite in Rocky Arroyo; both facies are heavily fractured (6-ft geologist for scale).

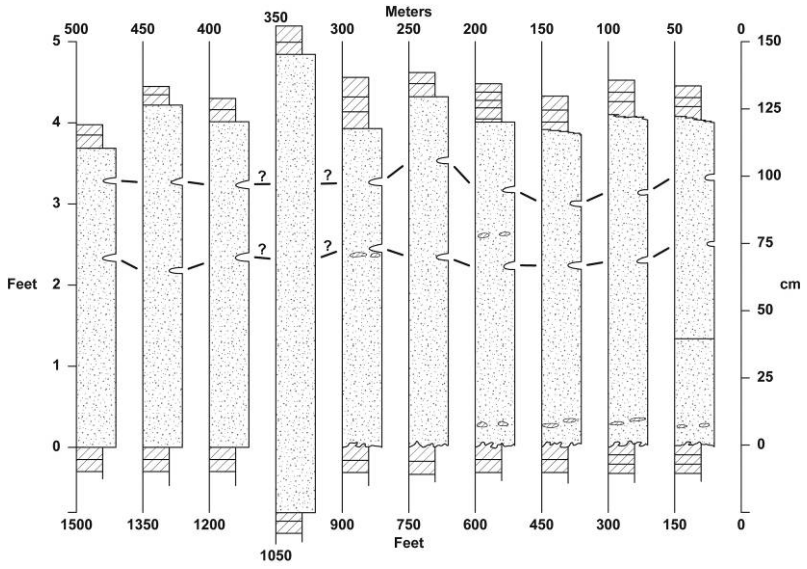

Figure 2.11 Measured sections through the most continuous bed at Rocky Arroyo. A photograph of the thickened sandstone in the fourth section in from the left can be seen in Figure 2.12. The thickened area is a cliff face and the location or even presence/absence of the two bedding breaks that are so prominent in the other sections cannot be determined.

Total bed thickness varies only slightly (between 3.9-4.6 ft; 1.2-1.4 m) across its exposed 1400 ft (425 m) extent, with the exception of a local swelling of the bed to approximately 5.6 ft (1.7 m) near the west end of the outcrop (Figures 2.11, 2.12). The thickened zone is exposed in a cliff face and could not be studied in detail, but it appears to fill a local depression associated with a facies change in the underlying beds, and its top seems to rise above the local bedding, possibly as a partially preserved dune form. The immediately overlying dolomite beds loose continuity over the top of this swelling, suggesting that water depth changed and that the dolomite was not deposited there.

Figure 2.12. Thickening of bed at horizon "A-A" above the geologist's head. Another sandstone bed at the level of the geologist's head terminates in a wedge immediately to his left.

Regardless of origin, this thickening represents an anomaly in the homogeneity of the most extensive and uniform of the sandstone beds present in the outcrop. The swelling is not unique: similar features are present in several other of the outcrops studied. The structures are important reservoir heterogeneity considerations.

A second sandstone in this outcrop varies from about 4.9 to 6.5 ft (1.5-2 m) thick. Although it can also be traced as a generally sandy horizon along the entire distance of the outcrop, terminated east and west by erosion, it grades into a sandy dolomite near the middle of the outcrop, thus it represents two separate reservoirs at the same horizon, one present for about 400 ft (122 m) at the west end of the outcrop, the other present at the easternmost 700 ft (213 m). The internal facies change would be a barrier to fluid (CO_2) flow between the two reservoirs.

A thin (half-meter thick) third sandstone extends only 300 ft. (90 m) It occurs several meters stratigraphically below the bed just described and centered below its non-reservoir interval, suggesting a sedimentary relationship. This small bed grades east and west into dolomitic, non-reservoir facies.

A fourth sandstone terminates westward with an abrupt, wedged bedding surface (Figure 2.12) that may represent the lee slip-face of a dune. This face is on lapped by a dolomite unit. The

sandstone can be traced eastward from this contact about 500 ft (152 m) before being obscured by cover. However, it does not appear in the section that re-appears above the arroyo bed to the east, and thus it probably terminates by facies change to dolomite, and is about 800 ft (245 m) in total lateral extent.

The fifth sandstone, a compound unit of two superimposed beds, is about two and a half meters in total thickness, and is only exposed for 600 ft (183 m) in hollows along the bottom of the arroyo near the east end of the exposure. It terminates east- and westward under cover, but is not present in the section where it resurfaces above a talus zone to the west, so it must terminate by lateral facies change within the talus zone and is probably about 1000 ft (305 m) in minimum lateral extent.

The sixth sandstone is also relatively thick (a doublet of two meter-thick sandstones), but is only exposed for about 300 ft (91 m) at the western end of the exposure, terminating westward behind brush and talus, and eastward under the floor of the arroyo.

Table 1. Lateral extents, heights, and terminations of sandstones in Rocky Arroyo

Western termination	Measured extent (ft)	Eastern termination	Max thickness (ft)
X	400	Z	4.9
Z	700	X	6.1
X	1400	X	5.6
Z	300	Z	1.6
Z	800	Z	3.3
Z	1000	X	8.0
X	300	X	6.6

X = covered or eroded end
Z = known termination by facies change

Ranging from 300 ft (91 m) to at least 1400 ft (427 m; Table 1), the minimum average lateral extent of these seven sandstones is 700 ft (213m). Six, or almost half of the terminations are not facies changes but are unknowns (erosion or covered), and the measured lengths of those beds with unknown terminations are only a minimum, therefore the actual average lateral extent maybe twice the minimum average, or on the order of 1500 ft (457 m).

The well-pair correlation data, described in Section 2.5 of this paper, suggest that at least half of the composite sandstone reservoirs have lateral dimensions of less than 1700 to 2500 ft (518 to 762 m). Given the limited data, the likely error bars on the data, and the difference that the outcrop beds are inter-bedded with dolomites at the top of the Queen Dolomite as discussed above, the outcrop and subsurface data sets are compatible.

(c) 2.3.2. Hillside Sandstone Outcrop (northwest quarter of the southwest quarter, section 29, T. 21 S., R. 24 E.)

The main body of the Shattuck Sandstone is partially exposed in a steep hillside half a mile to the southeast (Figure 2.13). This hillside, about 60 ft (18 m) high and 250 ft (76 m) wide, is

composed predominantly of sandstone. It is stratigraphically higher than the outcrop just described, and equivalent to the sandy lower Shattuck reservoirs at the West Pearl Queen field. The sandstones are again well sorted and very fine grained. However, bedding is thinner, the thick sandstones being composed of tabular beds 10 cm to a meter thick.

Figure 2.13 Sandy hillside of moderately well exposed Shattuck sandstone. Bedding appears to be uniform but local heterogeneities exist. The arrow marks a block of sandstone float that can be seen in the following photo and used for position reference.

A major permeability discontinuity is present in the hillside, in the form of a 12-ft (3.6 m) thick, 90-ft (27 m) wide sandy unit bounded on the bottom by what appears to be a Permian, syn-sedimentary erosion surface (Figure 2.14). One plausible interpretation is that it is a channel cut into the tabular beds by a high-energy event, possibly during a storm or flooding. The tabular beds at the margins of the channel have been truncated, and a zone of iron concretions has been cut out, with similar concretions present at the base of the lens, possibly as a winnowed lag deposit. However, incongruously, the channel was subsequently re-filled with the same type of low-energy, thin, tabular sandstones that it was cut into (Figure 2.15). Wavy, low-angle, and horizontal bedding as well as small ripples are preserved locally, suggesting low-energy depositional conditions, probably eolian deposition during dust storms, reworked by gentle currents. The channel axis is estimated to be northwest-southeast, or roughly normal to the local paleoshoreline.

Figure 2.14. Right-hand half of the channel form (diagonal contact from upper right to lower left) in the sandy hillside. The upper arrow marks the block of sandstone float used for a position reference between this and the previous photo (Figure 12); the lower arrow shows the position of the following photo.

Figure 2.15. High-energy, erosion channel-margin contact between low-energy flat-lying sandstones of the substrate on the right and low-energy inclined channel-filling sandstones on the left. A mirror image of this relationship is present on the other side of the channel 100 ft (30 m) to the northeast.

(d) 2.3.3. Teepee Arroyo (southwest quarter, section 29, T. 21 S., R. 24 E.)

The Shattuck sandstone proper is reasonably well exposed, although only in vertical section rather than in wide-scale lateral exposures, in a narrow arroyo that lies just southwest of the conical hilltop of Seven Rivers Formation called "The Teepee" on the local topographic maps. The Shattuck sandstones in this arroyo show a variety of depositional environments, including many of the typical meter-thick, apparently massive sandstones and inter-bedded thin dolomites. Sedimentary structures such as low-angle cross beds, small trough cross bedding, rare rippled bedding surfaces, and inter-bedded dolomites, again suggest low-energy, shallow-water deposition.

Other deposits exposed in this arroyo include a meter-thick intraclast conglomerate (Figure 2.16). The conglomerate has an irregular base and overlies deformed shale, suggesting rapid emplacement on top of an unconsolidated bed. The conglomerate is overlain by a horizontally bedded dolomite. The deformed underlying shale and the ripped-up intraclasts indicate a high-energy event, and this is probably a storm deposit, possibly related to the high-energy event that cut the channel in the sandy hillside just described.

Near the top of the arroyo, though well below the evaporitic deposits of the Seven Rivers Formation that overlies the Shattuck Sandstone, another ambiguous sandstone swelling is present. Thickening from 3.3 to 5.2 ft (1.0 to 1.6 m) and then thinning back to 3.3 ft (1.0 m) over a lateral distance of 33 ft (10 m), it overlies a storm-deposit bed of intraclast conglomerate, the top of which is depressed to accommodate about half of the swelling (Figure 2.17). The rest of the swelling is accommodated by an increase in height of the top of the bed. It is capped by a thin, uniformly thick dolomite. The geometry suggests that the underlying strata were poorly consolidated and bowed down slightly to accommodate the local weight of the sand thickening, and that topographic relief existed on the top of bed at the time that the overlying dolomite was deposited.

Figure 2.16. Intraclast conglomeratic storm deposit, Teepee arroyo.

Figure 2.17. Thickened tan-orange sandstone, possibly a drowned, isolated sand dune.

This example and others like it may represent isolated dune forms that were caught by rising sea level as they migrated across a barren shelf, their sharp dune form becoming subdued as they slumped during saturation with water, eventually becoming draped by later deposits. Other fossilized dunes should be present along the same horizon but it cannot be traced out laterally.

(e) 2.3.4. Eastern cutbank, Rocky Arroyo; (central part, section 29, T. 21 S., R. 24 E.)

The lower valley wall on the south side of Rocky Arroyo cuts straight northeast-southwest across section 29, extending into the northwest corner of section 28. The hillside exposure of Shattuck sandstone described previously (#2; Hillside Sandstone Outcrop) forms the southwestern end of this band of outcrops. The upper part of the Queen Dolomite and the lower part of the Shattuck Sandstone are intermittently exposed in this wall for over a mile, although individual beds cannot be traced laterally since the bedding dip varies, because the inter-bedded dolomites are too thin to protect the sandstone section from weathering, and because several arroyos interrupt bedding continuity. However, in addition to good fracture pavements (Figure 2.18) and the normal inter-bedding of dolomites and well-sorted, fine-grained sandstones, several features are present that affect bedding extent and continuity.

One notable feature is a small thrust fault in the northwest corner of section 28, a hundred yards east of the road that crosses the arroyo. Unmapped on the available geologic maps of the area, the fault plane strikes approximately NW-SE (Figure 2.19). Vertical displacement is on the order of 15-20 ft (4.6-6.1 m). Breccia zones are present along the fault plane, and also in between bedding planes in the eastern buttressing block where they resemble injections and suggest that the strata may not have been fully lithified at the time of thrusting.

Figure 2.18. Numerous natural fractures cut a bedding-plane fracture pavement.

Figure 2.19. Small thrust fault in the Queen Dolomite, Rocky Arroyo.

The thrust fault is located within half a mile of a mapped, accurate zone of small anticlines, but the orientation of implied compression (NE-SW) is nearly at right angles to the compression suggested by the anticlines (ESE-WNW in this area), and the two are not mechanically compatible and are therefore probably not related. The compression implied by the fault is, however, compatible with compression that would have been derived from faulting along the Huapache Monocline, a deep-seated thrust that strikes NW-SE about three miles to the southwest.

Although the West Pearl Queen Field is not close to a large structure that would be a source of compression, small subsurface faults similar to this thrust fault cannot be ruled out with the available data. In fact, although rare, other, smaller faults (Figure 2.20) are present elsewhere in the outcrop strata. Faults would be major barriers to fluid flow in a reservoir.

Figure 2.20. Small thrust fault in Rocky Arroyo. Thinning and thickening of the unit overlying the fault indicate that it formed during deposition.

In addition to subtle structural complexities (variable dip, thrust faulting), sediment logical heterogeneities complicate the reservoir-type strata in the Shattuck sandstones in this area. Another sandy thickening is partially exposed at the base of one outcrop. The bottom of the thickened sandstone is covered below the dry stream bed, but the top of the sandstone has 3 ft (1 m) of relief in the form of two subtle, connected mounds present along the 45 ft (14 m) of lateral exposure of the bed. The layers of sandstone and dolomite that immediately overlie these mounds conform to the double-mound topography, but the successively overlying layers thicken

in the troughs and thin over the high points such that bedding 10 ft (3 m) above the mounds is completely flat-lying. The mounds are again inferred to be small drowned sand dunes.

2.4 Summary

The observations on heterogeneities and the measurements of the lateral extents of reservoir-type sandstones in outcrop are compatible with and corroborate the inferences on limited reservoir dimensions made from subsurface data at the West Pearl Queen field to be discussed in the following section. Sandstone outcrops in the area of Rocky Arroyo were deposited in eolian and shallow lagoon environments. Heterogeneities such as facies changes, local bed thickenings, intraclast conglomerates, channels, and thrust faults interrupt lateral continuity of bedding and would effect the distribution of CO_2. Measured sandstone beds have an average minimum extent of 700 ft (213 m), but actual average extent is likely more, on the order of 1500 ft (457 m). Limited reservoir extents and internal baffles by heterogeneities of the types seen in outcrop may explain the anomalies, such as low CO_2 injection rates, the higher than expected injection pressures, and the observed lag in interwell communication, observed during injection of CO_2 in the West Pearl Queen carbon-dioxide sequestration project.

2.5 West Pearl Queen Field Assessment of the Lateral Extent of Permeability Units within the Shattuck Sandstone

This study was undertaken in order to assess the continuity of reservoir sandstones of the Shattuck Member of the Queen Formation at the West Pearl Queen field (Figure 2.21). Part of this study included an assessment of the depositional environment of the Shattuck sandstones, since sand bodies deposited in marine vs. non-marine environments would be expected to have different lateral extents and reservoir characteristics, and in order to make valid interpretations of the geophysical-log signatures. This environmental study included three cores, although only 20-30% of each core was available for examination due to extensive previous sampling and the absence of depth markings on one core caused some ambiguity. The core study was supplemented by an earlier outcrop study and literature search, and suggests a dominantly non-marine setting, in line with the previously published interpretations (Lorenz pers. com. 2006; Mazzulo et al., 1991, Tait et al., 1962; Hayes and Koogle, 1958).

The Shattuck Sandstone as defined here lies above the Queen Dolomite and below a widespread sandstone marker layer (Figure 2.22). This interval is between 64 and 106 ft (19.5 and 32.3 m) thick on the cross sections constructed for the study, thinner to the north and northeast (landward) and thicker to the south where greater subsidence apparently accommodated greater deposition (Figure 2.23). Lithofacies in the cores suggest that the sandstone reservoirs in the West Pearl Queen area were deposited in saline sand flats ("sabkha"), eolian dunes, and inter-dune environments (Figure 2.24). There may also have been some marginal-marine influence, especially in the lowest strata immediately adjacent to the Queen Dolomite and in the higher part of the Shattuck section.

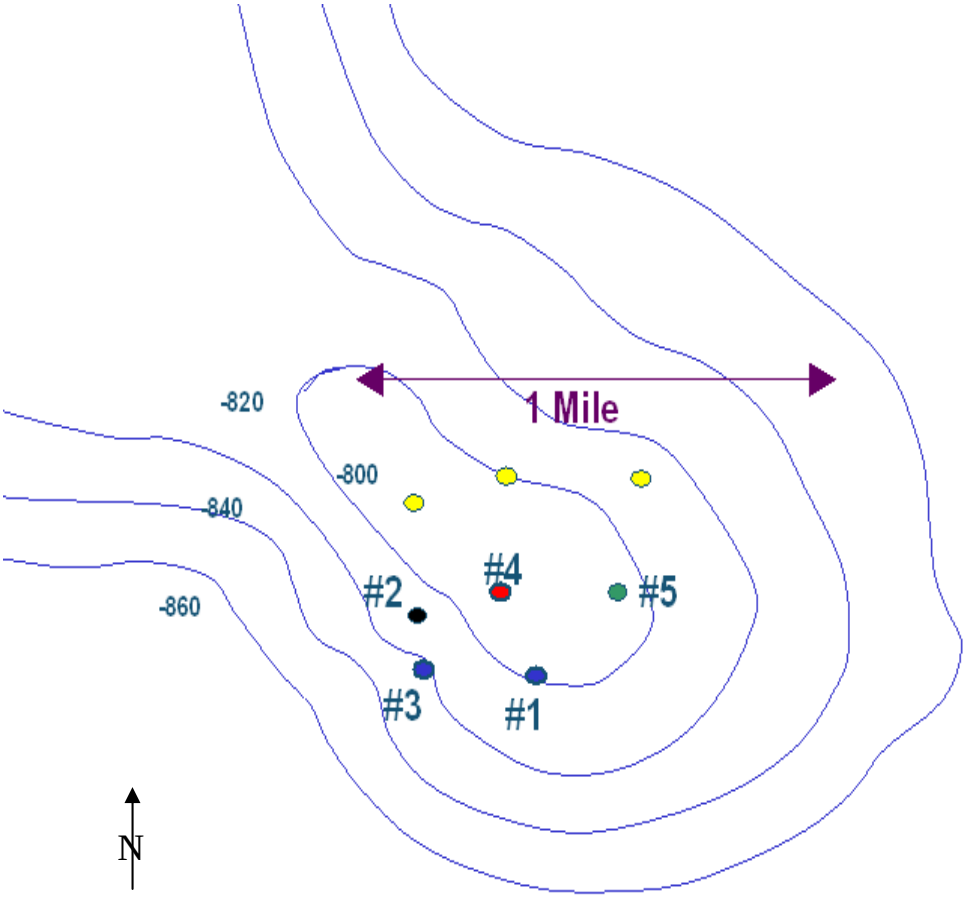

Figure 2.21. Structure-Contour map of the West Pearl Queen field, based on well data (compare to the different structure-contour map derived from the seismic data, Figure 28). Colored circles are the wells of different operators in the field; wells #4 and #5 are the injection and observation wells, respectively, and well #1 was cored.

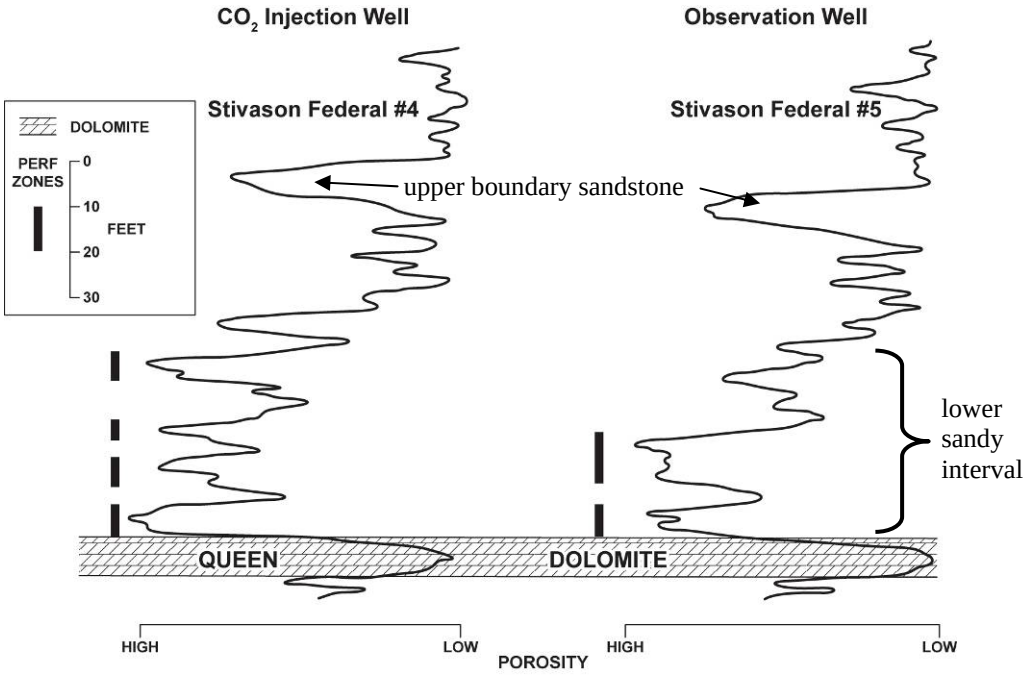

Figure 2.22. Neutron porosity log traces for the Stivason Federal #4 (CO2 injection well) and Stivason Federal #5 (monitoring/observation well). This figure shows the persistent Queen Dolomite bed that anchored the cross sections and well pairs, the laterally extensive sandstone that marks the upper boundary of the study interval, the relatively sandy lower part of the Shattuck interval vs. the finer-grained upper part, the limited zones of perforation in each well, and the thinning of the section in the direction of the Stivason Federal #5 well.

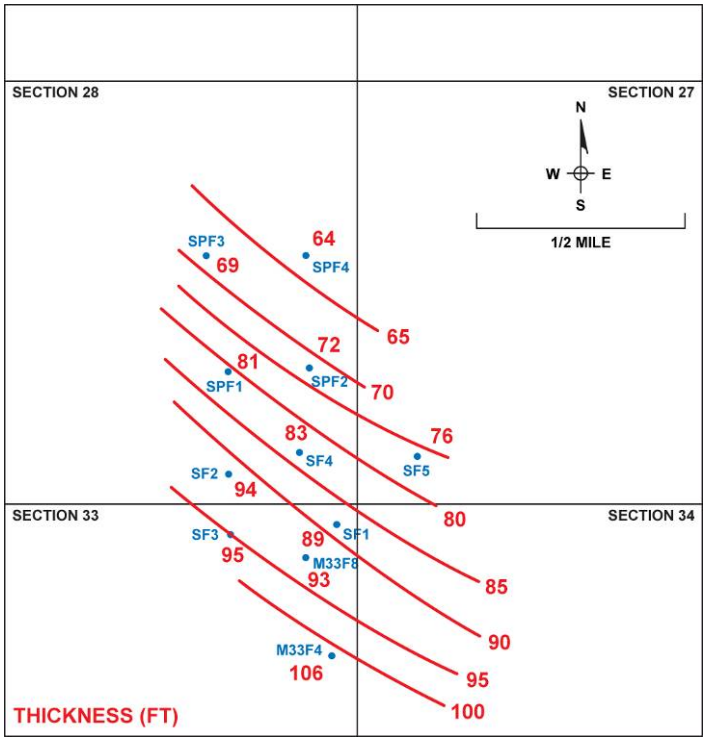

Figure 2.23 Isopach map of the Shattuck sandstone interval, between the top of the Queen Dolomite and the top of the upper, laterally-extensive, bounding sandstone. The interval thickens to the southwest, down dip, by 42 ft (12.8 m; an added 66%) over the short interval mapped. This thickening had to be accounted for in assessing the probability of bed correlations between wells. Wells SF4 and SF5 in sections 27 and 28 are the injection and observation wells, respectively, near the center of the West Pearl Queen field. Small blue letters are abbreviations of the well names, and red lettering shows the thickness of the Shattuck interval in each well.

High-porosity sandstone beds that form reservoirs capable of accommodating injected CO_2 within the Shattuck interval comprise only 30-40% of the total thickness of the unit, the rest being composed of low-porosity; well-cemented siltstones and local muddy and carbonate intervals. Five such beds and approximately 36 ft (11.0 m; cumulative) of reservoir-potential sandstone thickness are present in the Stivason Federal #4 CO_2-injection well. However, the operator perforated a cumulative of only 22 ft (6.7 m) of vertical height the casing in this well (in the four most promising oil-bearing zones: see Figure 2.22), leaving approximately 14 ft (4.3 m) of potential reservoir sandstone behind casing and unavailable for CO_2 injection.

The reservoir sandstones vary from single beds between 2 and 6 ft (0.6 and 1.8 m) thick to compound sandstones up to 16 ft (4.9 m) thick. The lower half of the Shattuck interval has a higher percentage of sandstone, and the compound sandstones in this zone form laterally persistent sandy intervals. The individual beds that comprise these sandy intervals cannot be reliably correlated and probably do not extend between wells. The questions are 1) how well interconnected are the individual beds within the sandy intervals, and 2) what are the likely lateral dimensions of the sandstones and sandy intervals. A lack of lateral reservoir continuity

between the wells, especially if combined with a lack of vertical conductivity between the component beds in the sandy zones, would help to explain the injection anomalies.

Figure 2.24 Steeply inclined, regular cross bedding of well-sorted, fine-grained sandstone, representing the deposits of an eolian dune environment, as seen in core. One of the bedding planes is highlighted by gray discoloration, suggesting enhanced permeability along this plane. The overlying gray bedding is nearly horizontal and on laps the inclined dune foresets.

Figure 2.25. Evaporitic nodular anhydrite that grew displacively in a fine-grained saline sandflat to sabkha environment.

(f) 2.5.1. Methods

Two approaches, 1) correlations along several cross sections, and 2) correlations between 21 well pairs, were used to semi-quantitatively assess the lateral continuity and extents of the permeability units that control distribution of CO_2 injected into the Shattuck sandstones. The correlations were based in part in the log similarities as described below and in part on knowledge of depositional environments.

(g) 2.5.2. Cross Sections

Four cross sections were constructed through the Shattuck interval in the area of the West Pearl Queen field. A three-mile long cross section extends between 11 wells in a generally north-south direction, approximately parallel to the depositional dip. Three shorter, orthogonal cross sections, each extending parallel to the northwest-southeast depositional strike, were also made (Figure 2.26).

Sections were referenced to the Queen Dolomite, a 6 to 12 ft (1.8 to 3.6 m) thick unit that provides a prominent and easily recognizable marker at the base of the Shattuck Sandstone. This dolomite has a distinctive, low gamma-ray/low porosity geophysical-log signature, and is also prominent outcrop as a highly fractured unit (Figure 2.27). It was deposited in a wide-spread, shallow, hyper-saline lagoon setting, and provides a good stratigraphic marker. The subsurface sections were constrained at the top by laterally-extensive, distinctive sandstone that is 5 to 10 ft (1.5 to 3.0 m) thick within an otherwise low-porosity zone.

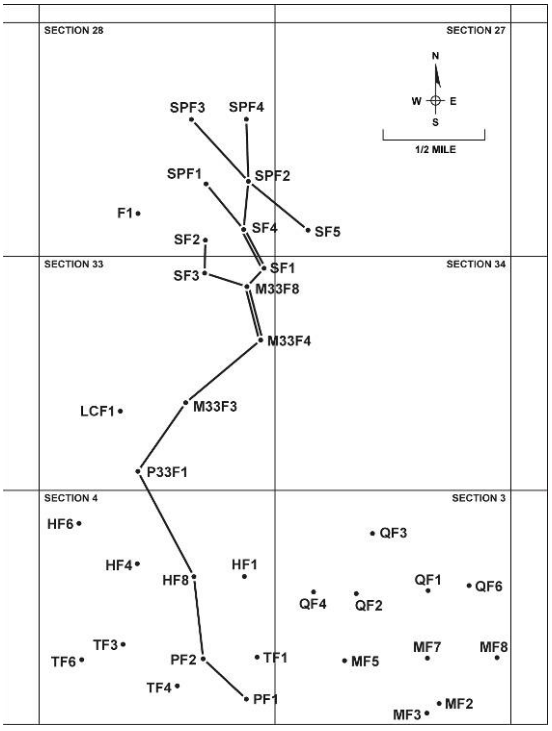

Figure 2.26. Map showing the lines of the cross-sections constructed for this study. Double lines show where a section is part of both the long, north-south section and one of the oblique sections. Lettering indicates the abbreviations for well names. SF4 and SF5 in sections 27 and 28 are the injection and observation wells, respectively.

Figure 2.27 Outcrop of the Queen Dolomite, with a yellow, 5" x 7" field notebook for scale. This unit is well bedded and heavily fractured, and forms a persistent layer that is easily recognizable in both outcrop and the subsurface and that can be used as a peg point for assessing correlations of the sandstones in the overlying Shattuck interval. Significant fracturing, if present in the subsurface, could also make this an important potential thief zone.

Gamma-ray logs proved to be useless for correlation purposes because a high potassium feldspar content of the Shattuck sands left little to differentiate the reservoir sandstones from the low-porosity, finer-grained clastic lithologies. However, distinctions between the lithologies were obvious on the density and porosity logs, which delineate the high-porosity units of prime interest for sequestration. An oilfield type of cutoff criterion was used in that only sandstones with more than 12% porosity were considered for correlations.

High-porosity sandstone units were assumed to extend between two adjacent wells if the following correlation criteria were met, listed in order of priority:
1. The position of the high-porosity sandstone is a similar distance vertically from the Queen Dolomite, although allowing for the gradual and regular thickening of the section to the southwest and the related progressively higher position of correlative beds relative to the underlying dolomite marker bed in this direction.
2. The shape of the porosity log profile across the two sandstones in adjacent wells is similar.
3. The possibly correlative sandstones in the wells have at least 12% porosity.

Sandstone that did not correlate between adjacent wells was assumed to pinch out half-way between the wells. The maximum inferred extents of the correlatable sandstones were tabulated and used to determine the maximum, minimum, and average extents along the north-south cross section. The same was not done for the east-west cross sections since they examined only limited

distances relative to the maximum sandstone extents observed on the north-south section, which would have provided only an artificially truncated data set.

(h) 2.5.3 Well Pairs

The second technique used for assessing the lateral extents of the Shattuck high-porosity sandstones was to make a comparison of correlations of sandstone units between 21 adjacent well pairs, the wells in each pair being separated by distances of between 500 and 1900 ft (152 and 580 m; Figure 2.28). These correlations also used the Queen Dolomite and the upper, extensive sandstone as the stratigraphic references, and used the same correlation criteria listed above.

The correlation pairs were also examined relative to paleogeography, i.e., by alignment northeast-southwest and northwest-southeast (across and parallel to the depositional strike respectively), as well as north-south and east-west (oblique to depositional strike), in order to see if sandstone continuity varied in these directions.

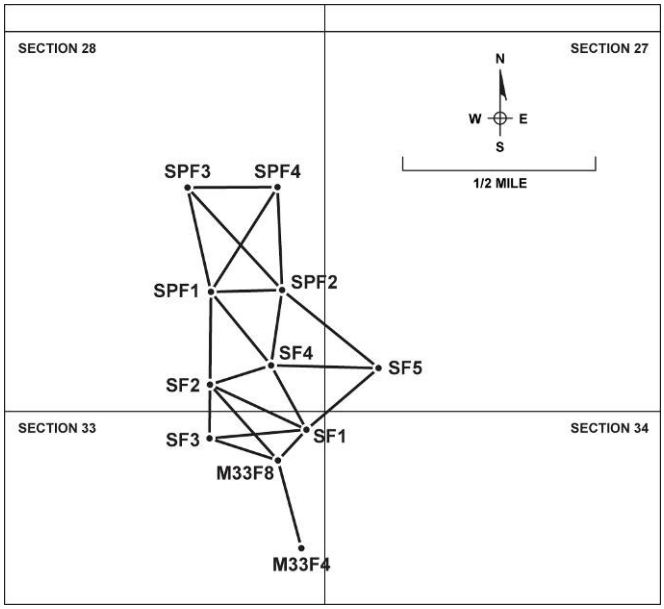

Figure 2.28 Map showing the well pairs used to derive correlation percentages. Wells SF4 and SF5 near the right center of the figure are the injection and observation wells, respectively, near the middle of the West Pearl Queen Field.

The percentage of total number of reservoir-quality compound sandstone packages in each well pair that appeared to correlate between wells was then plotted against the distance between the well pairs, with the expectation that the interwell correlation percentage would decrease as the distance between wells increases, thus providing a basis for extrapolating the probable lateral extents of typical reservoir units.

Vertical conductivity between individual beds within the compound sandstone packages, and between packages, was assessed by a qualitative examination of the porosity log traces, and

corroborated by the existing core-property measurements (porosity and permeability) available for core from the Stivason Federal #1 well.

(i) 2.5.4 Caveats

Without evidence such as documented fluid communication between wells or interwell seismic wave guides, it is not possible to say definitively whether similar-looking sandstones penetrated in two adjacent wells at the same depth are actually contiguous between the wells or whether the similarity in depth and log profile are merely coincidental. In future sequestration projects it would be valuable to run various tests to assess the interwell connectivity of reservoir units prior to injection.

Some Shattuck sandstone beds can be traced laterally in outcrop for a few thousands of feet, supporting the lateral dimensions derived from the subsurface data below even though the depositional environment of the Shattuck has changed in these more marine deposits exposed northwest of Carlsbad. Nevertheless, the subsurface interwell correlation percentages discussed below do drop off, albeit irregularly, with distance, supporting the inferred correlations.

The longest correlations inferred for this study, up to 2600 ft (792 m), between well pairs and along the north-south cross section, may be spurious, more apparent than real. Beds as little as a foot thick can be resolved in the porosity logs, but these could not be reliably correlated.

2.6 Continuity Interpretations

Rather than being discrete units that blanket the field in uniform layers, reservoir-quality sandstones in the Shattuck Member of the Queen Formation occur as groups of composite sandstones that form distinct sandy intervals (Figure 2.29). These intervals in each well are composed of between one and five individual sandstone beds, as inferred from minor inflections of the porosity log traces across the compound units. The sandy intervals typically, though not always, extend laterally between adjacent wells, but in the lower Shattuck interval of interest here, the individual component sandstones commonly do not.

The sandy intervals record widespread conditions and environments that were conducive to local sand deposition. The potential for fluid connectivity within the sandy intervals, between the component sandstone beds, is not well known. As discussed below, the indirect evidence suggests that the potential is not high.

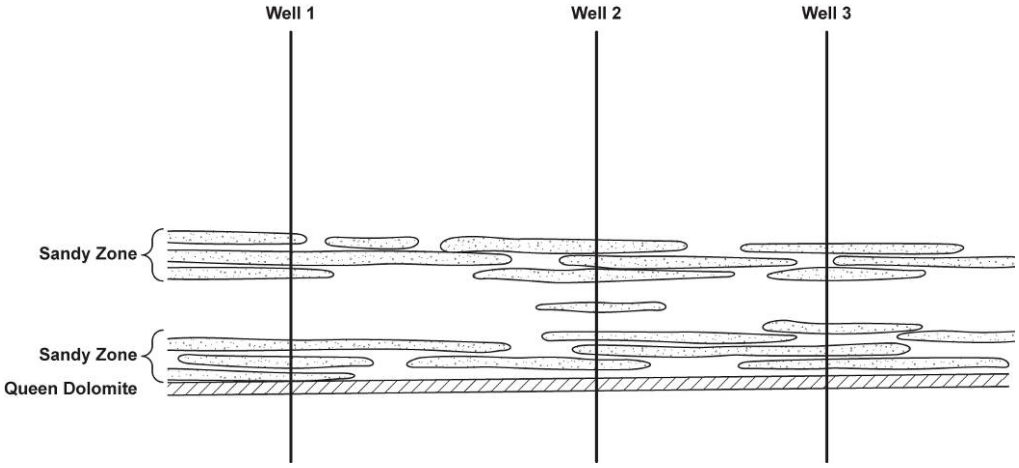

Figure 2.29 Schematic correlations between wells showing the interpreted nature of the sandstones in the lower Shattuck interval. The sandstones occur predominantly within sandy intervals that appear to correlate between wells but in fact the component sandstone beds are discontinuous. The individual sandstone beds that comprise the sandy intervals thin and thicken, and commonly pinch out between wells. Locally, even the compound sandy intervals themselves terminate and do not correlate.

(j) 2.6.1 Lower Shattuck Interval: Cross sections

Between three and six compound sandy packages, varying from 3 to 16 ft (0.9 to 4.9 m) thick, occur within the lower half of the Shattuck interval in the vicinity of the West Pearl Queen field. Core suggests that these sandstones were deposited in eolian dune and interdune intervals when the shelf margin was widely exposed as the sea retreated after deposition of the Queen Dolomite. Sandstones with reservoir potential that were deposited in these environments would not be expected to be as laterally extensive as the equivalent shallow-marine sandstones discussed in Part I that outcrop 60 miles (96 km) to the east. Dune fields developed above the water table, while briny sabkha environments filled the shallow depressions between dunes and between dune fields. The lower parts of dune deposits were preserved locally by rising water tables, or where a dune was blown into and across a sabkha and became stabilized by the precipitation of evaporitic cementing minerals.

Four of the five high-porosity sandy packages in the Stivason Federal #4 well were perforated in the injection well. The fifth interval apparently did not have promising oil indications on the geophysical logs and was not perforated by the operator when completing the well. Therefore some of the potential Shattuck CO_2-sequestration reservoirs penetrated by the injection well were not accessed during injection.

Twenty-one compound sandstone packages were identified within the north-south cross section. Some of the packages in the lower Shattuck interval were tentatively correlated as far as 9000 ft (2740 m) on the section. The average correlation distance was about 4000 ft (1220 m) and the minimum distance was less than 1000 ft (305 m). The sandy zones fan out and increase in number southward as the Shattuck section thickens: three sandy packages are present in the northern wells, whereas up to five packages are present in the southern wells.

(k) 2.6.2 Lower Shattuck Interval: Well Pairs

The graph of sandstone correlation percentage versus interwell distance for different pairs of wells in this lower Shattuck interval (Figure 2.30) does not show tightly grouped data from which general trends can easily be extracted, but it does suggest that all or most of the compound sandstone packages extend laterally for at least 1000 ft (305 m).

The percentage of interwell correlations, which can be used as a proxy for the probability of sandstone continuity, starts to drop off at distances greater than 1000 ft (305 m). Although there are still data points suggesting good reservoir continuity at distances up to 1900 ft (580 m) the maximum interwell distance plotted for the well pairs), the data also suggest that 20-30% of the sandy reservoir packages do not extend farther than 1500 ft (457 m). An empirical extrapolation of the trend suggests that only 50% of the sandy packages extend laterally for more than 2500 ft (762 m). This is consistent with the average correlation distance of 4000 ft (1220 m) derived independently from the cross sections.

Although the subsets of data are small when the well pairs are broken down by alignment relative to paleogeography, most of the alignment directions did not show distinctive differences. This supports the interpreted eolian-dominated depositional environment, where sandstone elongation trends would not have been controlled by position relative to the shoreline as might be expected of tidal-channel or lagoon deposits.

Three of the four data subsets show irregular trends of less correlation with distance, as expected. Only the seven data points for the subset that is oriented northwest-southeast, parallel to depositional strike (i.e., parallel to the paleoshoreline) do not show a trend where correlation percentages drop off with distance, suggesting instead an implausible trend of higher correlation with greater distance. This may be due to spurious correlations at greater interwell distances as suggested above; it is more likely these are simply similar depositional environments and not laterally continuous beds.

In fact, without this data subset, the remaining 14 data points show a more definitive and steeper trend of decreasing correlation with distance between the well pairs (Figure 2.31), suggesting that 50% of the sandy intervals may not extend laterally for more than about 1700 ft (518 m).

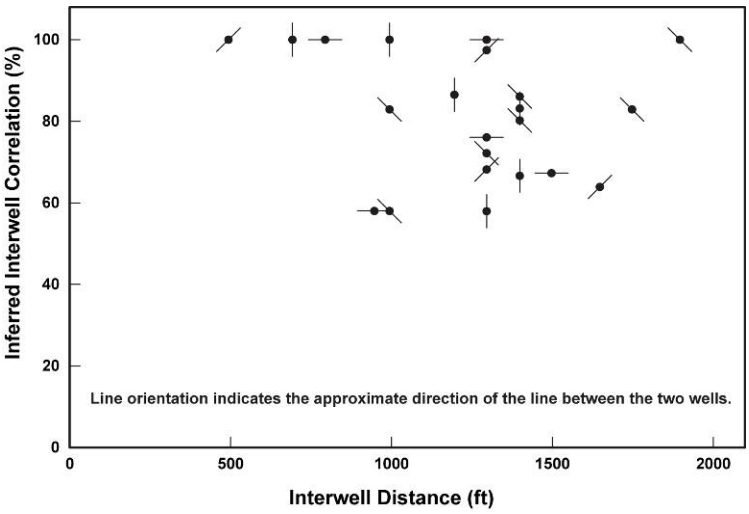

Figure 2.30. Chart of the distance between wells versus the percentage of sandy packages that correlate between two wells for each of 21 well pairs. The correlation percentage decreases irregularly with distance, suggesting limits to the lateral extents of the sandy zones. The approximate orientation of the line between the two wells for each pair is indicated by the orientation of the slash through the data point ("north" is up).

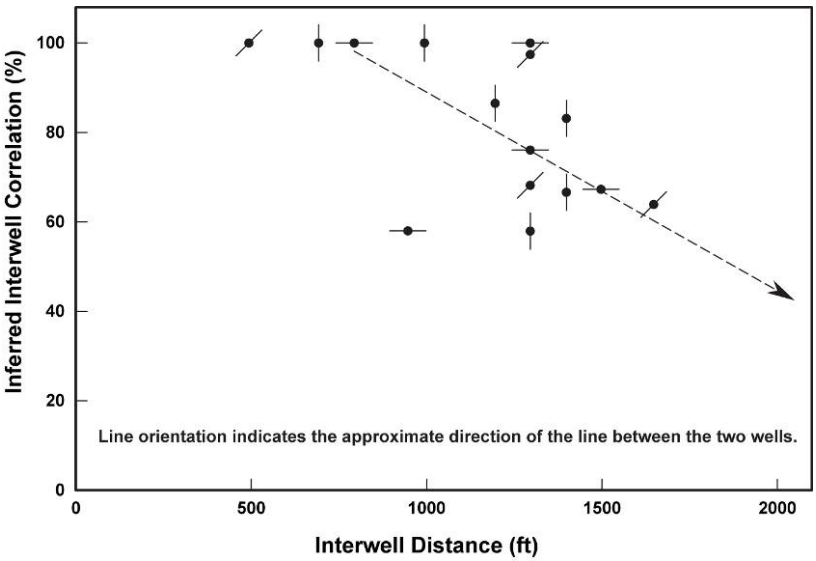

Figure 2.31. The restricted data set of those fifteen well pairs having all orientations except northwest-southeast. The dashed line is an estimated best-fit trend to the data points showing better alignment of the data into a trend of decreasing correlation with increasing interwell distance.

(l) 2.6.3 Reservoir Continuity and the Apparent Ponding of CO_2

The pre- and post-injection 3-D seismic results suggest that a bubble of CO_2 ponded at the base of the injection well (Figure 2.32). This, plus the higher than-expected-injection pressure (which necessitated an injection rate of only 40 tons per day rather than the calculated potential rate of

200 tons per day), suggests that the individual component beds of the Shattuck reservoir sandstones are not well interconnected, either laterally or vertically, and that even the compound sandstone beds are not laterally extensive.

The data on lateral continuity and interwell connectivity presented here suggest that fully half of even the compound sandstones extend laterally no farther than a few thousand feet. The radius of the mapped irregular CO_2 bubble is less than 1000 ft (305 m). The correlation of sandstones from the injection well to the five immediately adjacent wells are among the poorer correlations in the area, suggesting that the sandstones are more limited in lateral extent in this vicinity, possibly explaining this apparently restricted bubble of injected CO_2.

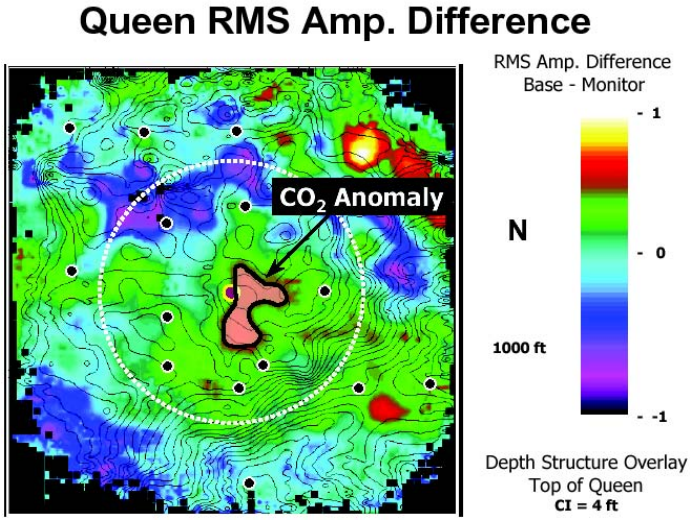

Figure 2.32. Three-dimensional seismic data showing the structure-contour map based on seismic data (black lines: compare to Figure 20a) and the interpreted CO2 anomaly location based on root mean squared (RMS) analysis of the data. The Stivason Federal #4 injection well is the purple dot at the left margin of the CO2 anomaly, and the Stivason Federal #5 observation/monitoring well is the first well to the east of the anomaly (north is up). Figure from Bob Benson, Colorado School of Mines.

A consideration is that the CO_2 bubble portrayed on the seismic map is two dimensional, whereas three and four separate, stacked, sandstone packages were perforated and presumably accepted the injected CO_2 in three dimensions. The seismic data do not have enough resolution to show CO_2 anomalies in each of the four injected reservoirs, therefore the seismic map shows the composite seismic response from the four zones, each in themselves being composed of smaller sand bodies, and each of which presumably has different lateral dimensions just as each has a different thickness.

The seismic anomaly may only portray the zone of maximum signal, where CO_2 is present in most or all four of the reservoirs. Individually, the four reservoirs probably extend further in different directions than the anomaly suggests. However, the observed high injection-pressure data argue that the reservoir extents are in fact limited, and that only a relatively small reservoir volume accepted CO_2.

None of the available data suggest that the reservoirs are limited structurally, but faults are not uncommon in the Permian basin and neither do the data rule out this possibility. In fact, the structure of the West Pearl Queen area is not well known: the seismically-derived structure map suggests a distinctly different structural configuration of the strata from the map constructed from well-log data (compare Figure 20a with Figure 28). Faults with vertical offsets of less than about 50 ft (15 m) would not be visible on the seismic data, yet a fault with only 10 ft (3 m) of throw would completely truncate most of the Shattuck reservoirs. A wrench fault would also truncate reservoirs but would have no vertical offset and thus even less seismic expression, nor would it show on a structure map based on well logs regardless of the magnitude of offset.

A fault would vitiate the reservoir-continuity estimations based on well data developed here, since it would truncate all reservoirs that it cuts. A small north-south fault located just west of the injection well would plausibly explain the asymmetric distribution of the anomaly, which is present only east of the injection well rather than radially symmetric around it, and truncated reservoirs would explain high injection pressures.

To date, no material-balance calculations have been carried out to test whether the area and volume of the mapped CO_2 anomaly are compatible with the injected gas volume and available reservoir volume. Another potentially useful approach would be to see if production and injection data support reservoir-engineering calculations that might indicate whether the reservoirs have apparent boundaries (faulted or otherwise) based on changes in the slope of draw-down and buildup curves.

A final consideration is that a small seismic anomaly was present in the vicinity of the inferred CO_2 injection anomaly in the pre-injection seismic data. The significance of this anomaly, and of its coincidence with the inferred injection anomaly, has not been addressed.

(m) 2.6.4 Perforation Limitations on Fluid Connections between Wells

As noted above, only four of the five reservoir-quality Shattuck sandstones penetrated by the Stivason Federal #4 injection well were perforated. The perforated intervals range from three to eight feet thick, correlative to the thicknesses of the associated sandy-zone reservoir packages. A correlation of sandstone packages between the injection and observation wells (Figure 2.33) suggests that the upper perforated reservoir in the injection well may correlate to much thinner sandstone in the observation well, but even if it does, it was not perforated in the observation well. It is limited in lateral extent, and the lack of perforations in the observation well precludes fluid transfer between wells in this zone.

The middle two perforated zones in the injection well may correlate to a single perforated sandstone in the observation well, i.e., either this zone has split and become two zones somewhere between the two wells, or there are three different reservoirs: two in one well and one in the other. The zones are probably poorly connected between the wells due to this sedimentary complexity.

Only the lowest sandstone package, immediately above the Queen Dolomite, has both apparently good correlation between the two wells and perforations in each of them. This six- to seven-foot

thick zone would be the most likely to be continuous and to thus have the capability to conduct fluid between the wells.

Thus, only a third of the perforations, and thus probably only a third of the injected CO_2, went into a reservoir that is arguably contiguous between the observation and injection wells. The $CO_2$was injected at pressures that were purposefully maintained below the formation fracture gradient, thus the CO_2 should have stayed in the injected reservoirs. It should not have been able to migrate vertically into the overlying reservoir that was perforated in the observation well.

Gasses from the production stream of the nearby Stivason Federal #5 well were monitored for composition, anticipating the breakthrough of CO_2, but none was observed until approximately three years after injection even though the well is only a quarter-mile to the east. Moreover, no changes in oil production that might be attributable to CO_2 injection were observed in this well during that time, also suggesting limited migration of CO_2 between injection and observation well, and therefore that interwell conductivity and continuity are not ideal even in the most promising zone.

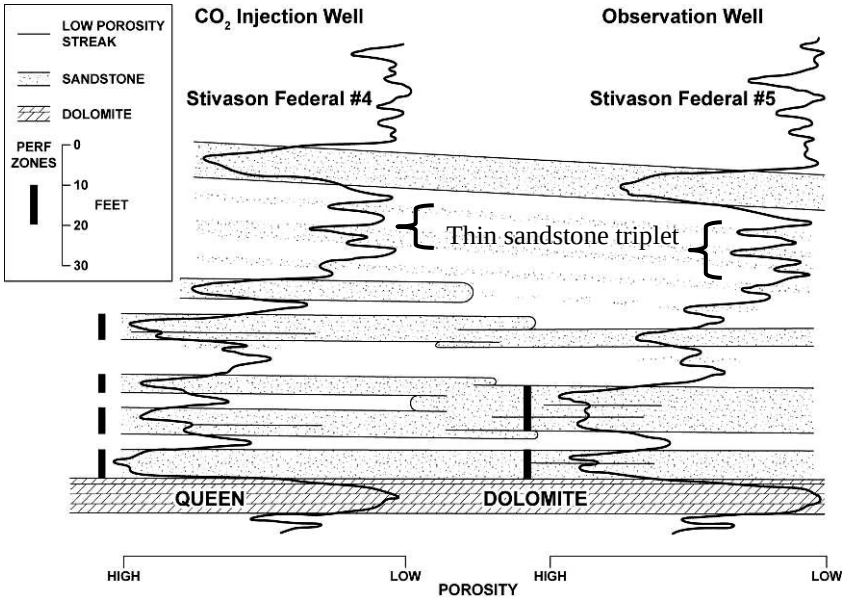

Figure 2.33 Interpreted correlations and continuity of Shattuck sandstones between one well pair: the Stivason Federal #4 (injection well), and the Stivason Federal #5 (observation/monitoring well) located approximately a quarter mile (0.4 km) to the east. Correlations of the non-reservoir sandstones in the upper part of the section are better, probably recording a shift to a more marine depositional environment. The Shattuck section is seven feet thicker in the injection well as a result of more subsidence and sedimentary accommodation space in this area.

(n) 2.6.5 Upper Shattuck Interval

The upper half of the Shattuck interval is predominantly fine grained and has low porosity. It contains thinner, individual sandstones, which, in the absence of core, cannot be definitively assigned to depositional environments. A distinctive triplet of thin sandstones in this upper

interval (Figure 2.33) appears to extend laterally between most wells in the study area, but they are not thick enough to be significant reservoirs and were not perforated. The thicker, uppermost sandstone that caps the Shattuck interval also correlates between wells, blanketing the area, probably as a result of rising sea level.

(o) 2.6.6 Vertical Conductivity between Beds

Core data and the geophysical porosity logs suggest that vertical conductivity was interrupted by thin, finer-grained, low-porosity zones that separate the component beds within sandy zones, as well as by the thicker low-porosity zones that are interbedded between those zones. Minor inflections of the geophysical log porosity traces across the overall sandy intervals record these low-porosity zones within the reservoirs.

Cores suggest that the low-porosity zones are commonly less than half a foot thick, thus the geophysical-log trace does not have time to record the appropriate low-porosity indication during the brief sensor passage time across these intervals while recording the logs. Nevertheless, they are significant baffles to vertical permeability within the system. Porosity and permeability data taken from core plugs of the finer-grained, non-reservoir intervals in the Stivason Federal #1 well (Figure 2.34) demonstrate that permeabilities in the non–reservoir intervals are too low to allow ready vertical communication between reservoirs. The lack of ready communication of CO_2 vertically between those reservoirs injected into in the Stivason Federal #4 well and the different reservoirs perforated in the nearby Stivason Federal #5 observation well supports the inference that vertical fluid communication was limited within and between these reservoirs.

The pores in the finer-grained beds between the reservoir sandstones are small, and they are commonly filled with cement, resulting in low permeabilities. Unless natural fractures exist to connect the reservoirs across the fine-grained intervals (and none have yet been observed in the limited core even though the outcrops are extensively fractured), fluids such as oil and/or CO2 would not have ready communication among or between the different Shattuck sandstones.

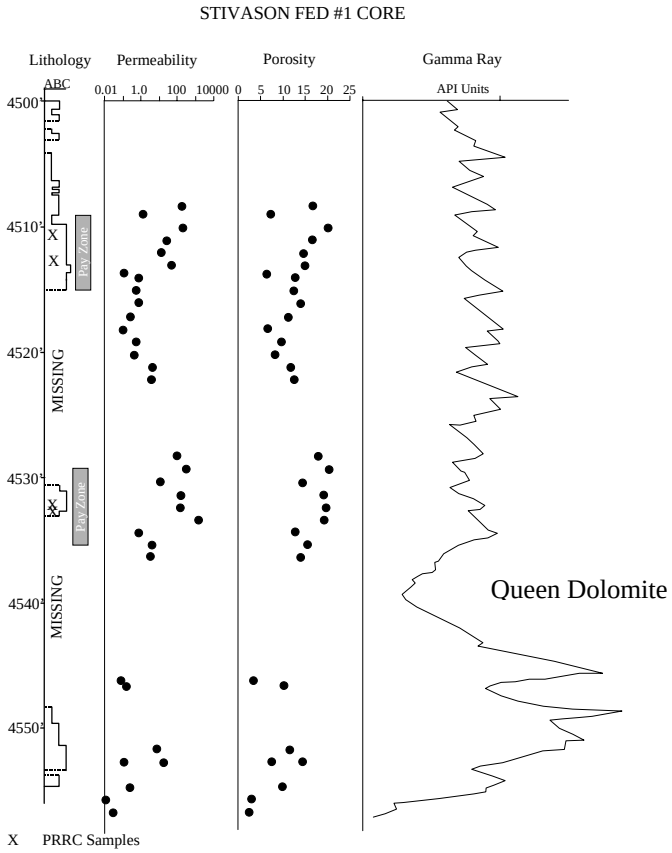

Figure 2.34 Porosity and permeability measurements from the Stivason Federal #1 core ("SF1" on previous figures) show that permeability drops below a millidarcy (and probably considerably less under in situ conditions of water saturation and stress) in the finer-grained intervals between reservoir sandstones, limiting vertical permeability within and across the reservoirs. Only two sandy packages had sufficient quality to be deemed "pay" zones by the operator in this well, even though it is only 1000 ft (305 m) southeast of the Stivason Federal #4 injection well where four sandy intervals had enough reservoir potential to have been perforated by the operator. This core extends below the Queen Dolomite, which is indicated by the low gamma-ray trace at about 4535-4544 ft (1382.2-1385.0 m). The high porosity/high permeability zone below the Queen Dolomite is irrelevant to the CO2 injection since it was not within the area isolated by packers during injection. A significant percentage of this core had been removed for sampling, study, and souvenirs (the "missing" intervals).

2.7 Summary

The higher-than-expected injection pressure (which necessitated an injection rate of only 40 tons per day rather than the calculated potential rate of 200 tons per day) and the 3-D seismic results which indicate a bubble of CO_2 ponded near the injection well, suggest that the individual component beds of the Shattuck reservoir sandstones are not well interconnected, either laterally or vertically, and that even the compound sandstone beds are not laterally extensive. This work analyzed the lateral continuity of the reservoir sandstones utilizing outcrop and subsurface data.

The observations on heterogeneities and the measurements of the lateral extents of reservoir-type sandstones in outcrop are compatible with and corroborate the inferences on limited reservoir dimensions made from subsurface data at the West Pearl Queen field. Sandstone outcrops in the area of Rocky Arroyo were deposited in eolian and shallow lagoon environments. Heterogeneities such as facies changes, local bed thickenings, intraclast conglomerates, channels, and thrust faults interrupt lateral continuity of bedding and would effect the distribution of CO_2. Measured sandstone beds have an average minimum extent of 700 ft (213 m), but actual average extent is probably significantly more, on the order of 1500 ft (457 m).

Although the sandstone reservoirs of the Shattuck member occur in distinct zones and although they superficially appear to correlate between wells, they are probably not uniform, vertically-stacked, successive layers of laterally-extensive sandstone, and they are probably not contiguous between wells except at the closest well spacing's. The maximum interpreted lateral extent of the sandy zones along the north-south cross section is 9000 ft (2740 m), but the lateral dimensions of most of these composite reservoirs were probably considerably less, and the larger inferred dimensions may be the result of apparent but spurious correlations.

Well-pair correlation data suggest that at least half of the composite sandstone reservoirs have lateral dimensions of less than 1700 to 2500 ft (520 to 760 m), depending on which data set is being used. Permeability drops to less than a millidarcy between reservoirs and at finer-grained sedimentary breaks within reservoirs, limiting vertical continuity within and between reservoirs. Limited reservoir dimensions and internal low-permeability baffles may explain the low CO_2 injection rates, the higher than expected injection pressures, the apparently small seismic anomaly related to CO_2 injection, and the observed lag in interwell communication.

The methods utilized in this paper to assess the lateral connectivity of reservoir rocks and to capture reservoir heterogeneities are applicable to other geologic sites and could provide a more thorough analysis of a reservoir before CO_2 injection is initiated.

3. SEISMIC NUMERICAL SIMULATIONS

3.1 Introduction

The West Pearl Queen (WPQ) field carbon dioxide (CO_2) sequestration experimental site is located near Hobbs, New Mexico. Baseline seismic reflection data were acquired in late 2002, prior to injecting ~2100 tons of liquefied CO_2 into a porous sandstone formation at ~1370 *m* depth. A second, post-injection seismic survey was acquired in mid-2003. All field acquisition conditions were nominally the same for both of these three-dimensional (3D) reflection surveys. The objective of this "time-lapse" (or 4D) seismic experiment is to detect and monitor the CO_2 plume at depth. Differences in the recorded seismic traces may be attributed to changing conditions in the sequestration reservoir induced by injection of CO_2. The purpose of the numerical simulations reported here are not to match the field data but determine appropriate analysis techniques to image the plume utilizing 4D seismic surveys. Even though we do not wish to match the field data, we used model parameters suitable for the WPQ site.

The injection of 2100 *tons* of liquid CO_2 into the WPQ site corresponds to approximately 1.9 million kilograms of CO_2. At the reservoir pressure the density of CO_2 is approximately $800\,kg/m^3$. Thus the $1.9\times10^6\ kg$ translates to a pore volume of $2381\,m^3$ in order to sequester the CO_2. The porosity and CO_2 saturation will determine the size of the CO_2 footprint.

Initial unpublished results indicated that, in order to create more meaningful results, future work should include a realistic heterogeneous reservoir model, better values of wave speeds and mass density variations due to CO_2 injection, and a target size consistent with the amount of CO_2 injected. In this report we consider two reservoir models, each determined by correlation lengths obtained by Lorenz and Cooper (Sec. 2 this report). Here we consider two different realizations of the random distribution of the P-wave speed, V_p, and mass density, ρ, throughout the reservoir volume. In Model 1 there is a low value of V_p (high porosity) zone surrounding an injection well assumed at the center of the model. In Model 2, a region of large values of V_p (low porosity) zone surrounds the injection well. In both models we assume that the CO_2 saturation ranges from 3 percent to 27 percent. Note the CO_2 saturation values were taken from the work of Pawar (private comm.) from his modeling of the WPQ reservoir conditions. The bulk of the CO_2 is contained in the 27 percent saturation region for both of our models.

3.2 Earth Model

The Shattuck Sandstone Member of the Artesia Group was the CO_2 sequestering formation for the WPQ experiment. This sandstone lies between the overlying Seven Rivers Formation and the underlying Queen Formation. Prior to the injection of the CO_2, various well logs were obtained that include sonic, density, and porosity. The logs were taken from the top of Yates Formation that sits on top of the Seven Rivers Formation to approximately to the base of the

Grayburg Formation that underlies the Queen Formation. We wished to simplify the V_p and V_s wave speeds and density model.

The earth model was constructed of five layers. The top layer is a zone in which the velocities and density linearly increase from the surface to the next zone or the Seven Rivers layer. Reasonable surface wave speeds and density were chosen from data previously collected in the area. Their associated linear coefficients were adjusted to ensure that the P-wave first arrival agreed with the collected seismic data and the material properties agreed with the wave speed and density log data. These logs also served to supply an average density and P- and S-wave speed for the following four layers: Seven Rivers, Shattuck Sandstone, Queen and the Grayburg. For a further simplification, we set V_s equal to $V_p/\sqrt{3}$. The model is shown in Figure 3.1. Details of the velocity distribution used in the Shattuck Sandstone are discussed below.

The Shattuck's properties (V_p and density) were randomized based upon a Von Karman distribution and scaled correlation lengths observed at outcroppings by Lorenz and Cooper (Sec. 2 this report). The percentage of background randomization chosen was based upon the range of values observed in the well logs resulting in a good correlation between the model variation and the logs.

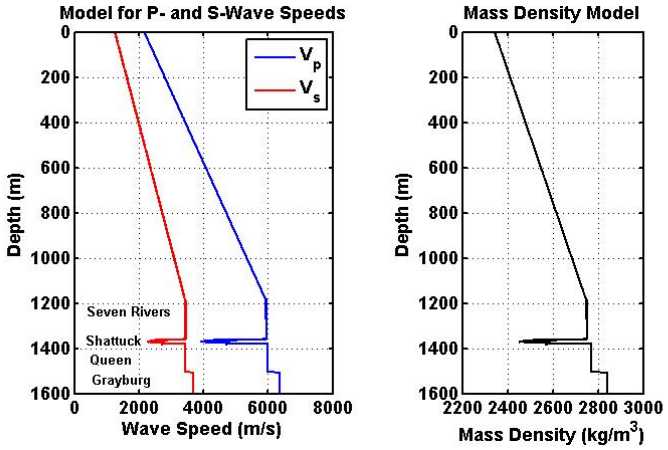

Figure 3.1 Model of the P- and S-wave speeds and the mass density.

In order to make a realistic heterogeneous reservoir, we consider two reservoir models, each determined by correlation lengths obtained by Lorenz and Cooper (Sec. 2 this report). For the first realization, Model 1, low values of V_p and hence high values of porosity ϕ surrounded the injection well. For the second realization, Model 2, we took high values of V_p (low porosity) that surrounded the injection well. V_p For both models prior to CO_2 injection at a depth of 1362 m are shown in Figure 3.2.

Han and Batzle (2004) gave a linear relationship for wave speeds as a function of porosity. Here we assume a linear relationship between V_p and the porosity ϕ such that

$$V_p = V_0 + a\phi\,. \tag{3.1}$$

Using the sonic and porosity logs from Stivenson #4 the linear fit to the data is shown in Figure 3.3. The fitting parameters are $V_0 = 6172\ m/s$ and $a = -16659\ m/s$. From the representative V_p distribution shown in Figure 3.3, we calculated a porosity as a function of *x*, *y*, and *z* using equation (1) as a function of position within the Shattuck sandstone.

$$\phi_{calc}(\mathbf{x}) = \frac{V_p(\mathbf{x}) - V_0}{a}\,. \tag{3.2}$$

Note: if $V_p(\mathbf{x}) > V_0$, we set $\phi_{calc}(\mathbf{x}) = 0$, since porosity cannot be negative.

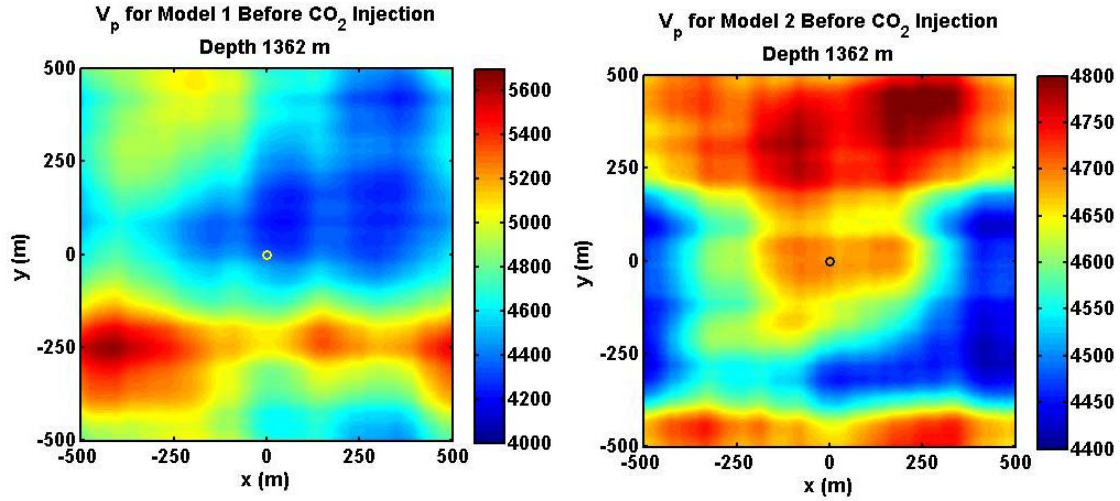

Figure 3.2 P-wave speed V_p for Model 1, left hand panel, and Model 2, right hand panel, prior to CO_2 injection at a depth of 1362 m. The location of the injection well is indicated at x=0 and y=0 m.

3.3 CO2 Storage

Having calculated a porosity surrounding an injection well, we determined the volume affected by the injection of liquid CO_2. The grid spacing for the seismic calculations is 2*m*, thus each grid node represents 8 cubic meters and the available pore space is the porosity times the 8 cubic meters. The amount of CO_2 stored in the 8 cubic meters is $8 \times \phi \times S_{CO2}$, where S_{CO2} is the CO_2 saturation. For both models, we assumed regions of 27 percent, 13 percent, and 3 percent CO_2 with saturations decreasing with distance from the injection well, where the bulk of the CO_2 is in the 27 percent saturated zone. In order to calculate the volume needed to store the CO_2, we calculated the pore volume in three concentric volumes, which we called boxes. The pore volume of each box is determined from summing the pore volumes at each seismic grid node within a prescribed *x*-*y* "footprint". Since the porosity distribution is different between the two models, the pore volumes of the so-called boxes will be different.

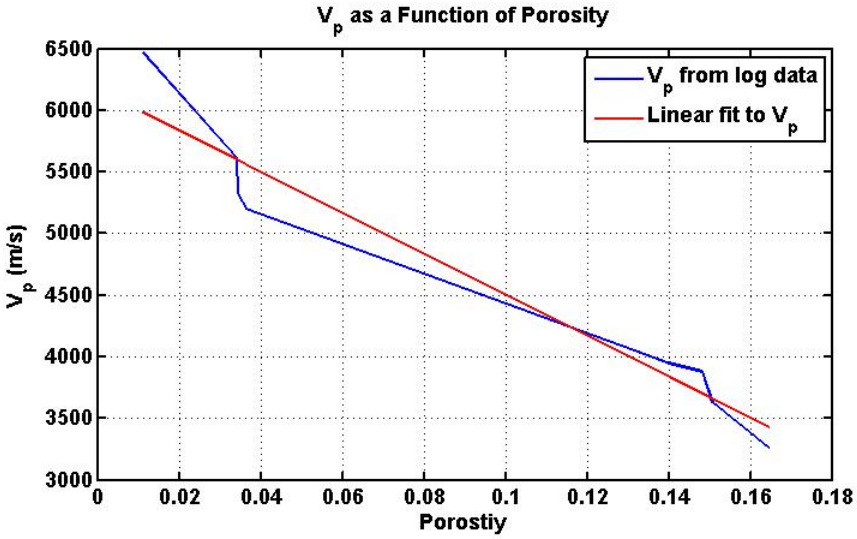

Figure 3.3 P-wave speed as a function of porosity with a linear fit to the well log data.

Model 1:

$$Box_1 = 8\times\sum\phi_{Model1}(x,y,z) = 6685\ m^3,\ -28\le x\le 28,\ -28\le y\le 28,\ 1360\le z\le 1378\,m$$

$$Box_2 = 8\times\sum\phi_{Model1}(x,y,z) = 11688\ m^3,\ -34\le x\le 36,\ -40\le y\le 40,\ 1360\le z\le 1378\,m$$

$$Box_3 = 8\times\sum\phi_{Model1}(x,y,z) = 15616\ m^3,\ -42\le x\le 44,\ -46\le y\le 42,\ 1360\le z\le 1378\,m$$

The volume of CO_2 is

$$Box_1\times 0.27 + (Box_2 - Box_1)\times 0.13 + (Box_3 - Box_2 - Box_1)\times 0.03 = 2373\ m^3$$

Which compares well with the pore volume of $2381 m^3$ calculated above needed to store the 2100 *tons* of injected CO_2

Model 2

$$Box_1 = 8\times\sum\phi_{Model2}(x,y,z) = 8092\ m^3,\ -34\le x\le 30,\ -44\le y\le 30,\ 1360\le z\le 1378\,m$$

$$Box_2 = 8\times\sum\phi_{Model2}(x,y,z) = 10796\ m^3,\ -38\le x\le 36,\ -52\le y\le 34,\ 1360\le z\le 1378\,m$$

$$Box_3 = 8\times\sum\phi_{Model2}(x,y,z) = 13846\ m^3,\ -42\le x\le 40,\ -62\le y\le 38,\ 1360\le z\le 1378\,m$$

$$Box_1\times 0.27 + (Box_2 - Box_1)\times 0.13 + (Box_3 - Box_2 - Box_1)\times 0.03 = 2385\ m^3$$

Again comparing well to the pore volume needed of $2381 m^3$

3.4 CO_2 Effects on Model Parameters

The introduction of CO_2 affects V_p, V_s, and ρ. The Gassmann (1951) equation calculates the bulk modulus of a fluid-saturated porous medium using the bulk modules of the solid rock matrix, the frame, and pore fluid. The Gassmann equation (*e.g.*, Wang, *et al.*, 1998) for the saturated bulk modulus K^* is

$$K^* = K_{dry} + \frac{\left(1 - \frac{K_{dry}}{K_s}\right)^2}{\frac{\phi}{K_{fl}} + \frac{1-\phi}{K_s} - \frac{K_{dry}}{K_s^2}}, \tag{3.3}$$

Where K^* is the bulk modulus of a rock saturated with a fluid with bulk modulus K_{fl}. K_{dry} Is the dry frame modulus and K_s is the mineral rock matrix modulus. ϕ is the porosity. The shear modulus μ is not affected by the pore fluid. For a water-CO_2 mixture we will take a Wood's average for the fluid bulk modulus (Wang, *et al*., 1998)

$$\frac{1}{K_{fl}} = \frac{1 - S_{CO2}}{K_w} + \frac{S_{CO2}}{K_{CO_2}}. \tag{3.4}$$

From Cooper, *et al*. (2008), the Shattuck Sandstone is made up of approximately 70 percent sandstone and 30 percent dolomite. The Woods average for the solid matrix Shattuck sandstone bulk modulus is $44.3\,GPa$ where the bulk module for sandstone and dolomite are $37.0\,GPa$ and $82.2\,GPa$, respectively.

From the original well log data (before introduction of CO_2) V_p, V_s, ρ and ϕ, we can calculate the original the shear modulus μ^0 and bulk modulus K^0 denoted by the super script 0. We assume that for the pre-injection data, $K_{fl} = K_w$ Thus in the unaffected reservoir (no CO_2) we have

$$\begin{aligned} \rho^0 &= (1-\phi)\rho_s + \phi\rho_w \\ \mu^0 &= \rho^0 V_s^2 \\ K^0 &= \rho^0\left(V_p^2 - \frac{4}{3}V_s^2\right) \end{aligned} \tag{3.5}$$

The shear modulus of the solid rock matrix is $\mu_s = \mu^0/(1-\phi)$. The mass density of the solid rock matrix, from equation (3.5), is

$$\rho_s = \frac{\rho^0 - \phi\rho_w}{1-\phi}. \tag{3.6}$$

The dry frame modulus K_{dry} can be determined from the pre-injection data setting $K^0 = K^*$ and $K_w = K_{fl}$ in equation (3.3).

For each nodal point in the CO_2 affected volume, we calculate the bulk modulus from equation (3.3) using equation (3.4) for the fluid bulk modulus. In addition we use

$$\rho_{sat} = (1-\phi)\rho_s + \phi\left[(1-S_{CO2})\rho_w + S_{CO2}\rho_{CO_2}\right], \tag{3.7}$$

to calculate the CO_2-affected mass density. The wave speeds and the mass density of the affected volume are

$$\begin{aligned} V_p^{CO2} &= \sqrt{\frac{K^*_{CO_2} + (4/3)\mu^0}{\rho_{sat}}} \\ V_s^{CO2} &= \sqrt{\frac{\mu^0}{\rho_{sat}}} \\ \rho_{sat} &= (1-\phi)\rho_s + \phi\left[(1-S_{CO2})\rho_w + S_{CO2}\rho_{CO_2}\right] \end{aligned} \tag{3.8}$$

For example, at a particular point in Model 1 and Model 2 before the introduction of CO_2, we have at $x = 0$, $y = 0$, $Depth = 1366\ m$

$Model\,1$	$Model\,2$
$V_p^0 = 4100\ m/s$	$V_p = 4770\ m/s$
$V_s^0 = 2367\ m/s$	$V_s = 2754\ m/s$.
$\rho^0 = 2477\ kg/m^3$	$\rho = 2674\ kg/m^3$
$\phi = 0.133$	$\phi = 0.0841$

For Model 1, the maximum and minimum porosities in the CO_2 affected zone are 0.137 and 0.072, respectively. For Model 2, the maximum and minimum porosities in the CO_2 affected zone are 0.094 and 0.009, respectively.

Using these model values at a starting point, Figure 3.4 shows the percentage changes in V_p, V_s, and ρ as a function of CO_2 saturation. The parameter changes for Model 1 are significantly larger than for Model 2 due to the larger value of porosity (lower values of V_p^0). The changes in V_s are due to the decrease in the mass density for increasing CO_2 saturation. Figure 3.5 shows a plan-view of the percentage change in V_p at the 1366 m depth with the obvious three CO_2 saturation zones: 0.27 (central), 0.13 (bordering the central region) and 0.03 surrounding the other two saturations. In reality, of course, the transitions between these saturation zones would be much more smoothed.

3.5 3D Numerical Simulations

The computational investigations of the CO_2 altered parameters are designed to quantitatively assess whether minute changes in the seismic reflection data can be recognized and properly

interpreted. Numerical models of the pre-CO_2-injection and post-CO_2-injection sequestration reservoirs, and synthetic seismic data were calculated for each case. Figure 3.6 shows the source and receiver locations for the numerical simulations. We used 17 sources and 147 receivers. The sources are vertical body force terms to simulate a vertical vibrator source and the receivers are vertical particle motion receivers (vertical geophones). We used a 25 *Hz* Ricker input wavelet giving dominant wavelengths between 160 m and 190 m. Grid spacing for the simulations is 2 *m*.

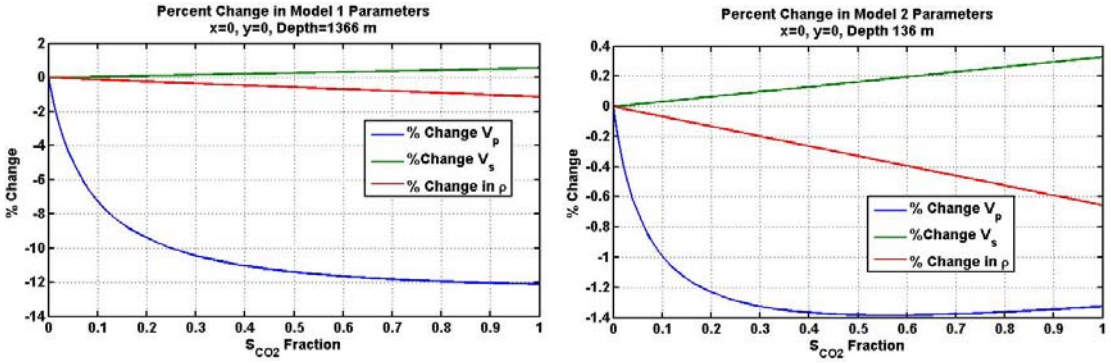

Figure 3.4 Calculated changes in V_p, V_s and ρ using Gassmann's equation for Models 1 (left-hand panel) and 2 (right-hand panel) as a function of CO_2 saturation. Locations are the same for both models.

The left-hand panel of Figure 3.7 shows calculated pre-injection traces minus the background traces. The source is at x=0 and y=-400 *m* and the receivers on a line from x=0, y=-400 *m* to x=0, y=400 *m* with an interval of 40 *m*. Here background traces were subtracted from the pre-injection traces to remove strong surface waves (ground roll). The background earth model was an extrapolation of the linear wave speed and mass density regime shown in Figure 3.1. The right-hand panel of Figure 3.7 shows the post-injection traces minus the pre-injection traces. Amplitude scale factors relative to unit source amplitude are indicted in the panels where the amplitude is the distance between traces. The amplitude of the post-injection traces minus the pre-injection traces is approximately five times less that the amplitude of pre-injection traces minus the background traces. The pre-injection traces (left-hand panel) display strong amplitude vs. offset for both the P-P reflections (~800 *ms*) and somewhat weaker the P-S and S-P reflections (~1000 *ms*). It is noteworthy that the P-S and S-P reflections are less prominent in the post- pre-injection difference traces (right-hand panel).

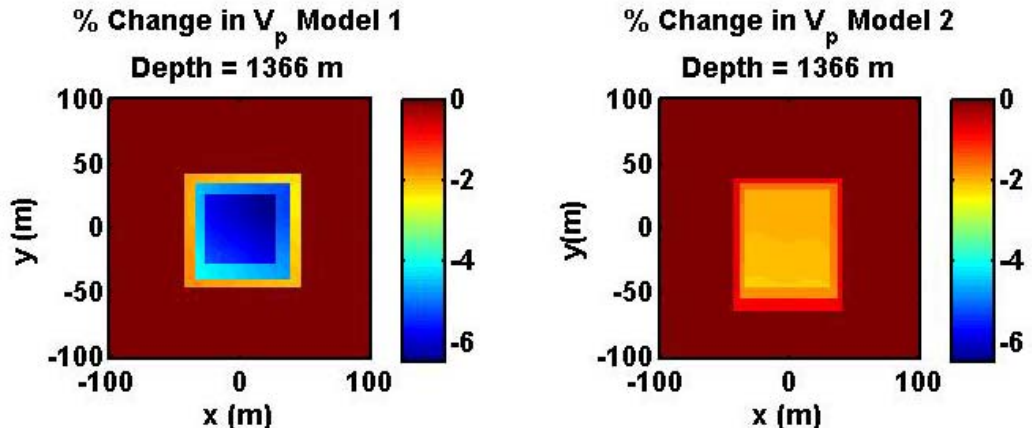

Figure 3.5 Percentage change in V_p at a depth of 1366 m for Model 1 (left-hand panel) and Model 2 (right-hand panel). Color scale is the same for both panels.

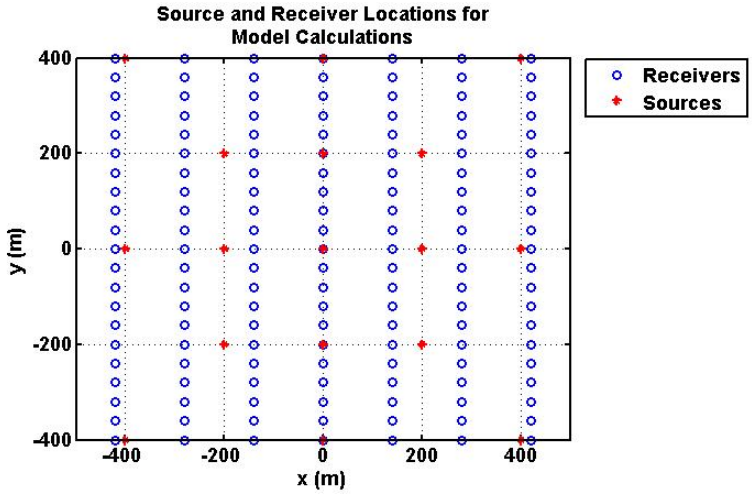

Figure 3.6 Source and receiver locations for the numerical simulations.

3.6 Data Analysis

The oil and gas exploration industry has long used migration of seismic data to image the subsurface. Seismic migration is the term for inverse wave scattering calculations that are used to move seismic trace reflection images to their location of origin, thereby producing an image of the subsurface. A commonly used migration method is Kirchhoff migration. As in all methods of seismic migration, Kirchhoff migration involves the back propagation (or continuation) of the seismic wave field from where it was measured into the region to be imaged. Continuation of the wave field requires a background model of seismic velocity, which is usually a model of constant or smoothly varying velocity and mass density. The implementation of Kirchhoff migration reduces to stacking the data along curves that trace the arrival time of energy scattered by image points in the earth. For a discussion of Kirchhoff migration, the reader is referred to Yilmaz (1987). In this report, we will focus on another migration method, namely the reverse-time migration (RTM) method (Bartel *et al.*, 2007). As with other types of migration, RTM requires a background model in which to back propagate the wave field in time to create a time-reversed wave field.

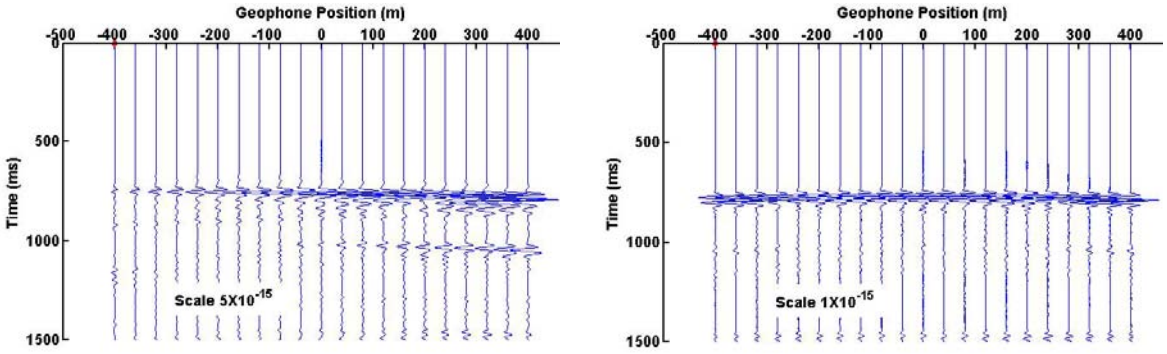

Figure 3.7 Trace samples from the numerical simulation for a line through the center of the model. The source is indicated by the red dot in the upper left-hand corner. Left-hand panel are the pre-injection traces minus the background traces and the right-hand panel are post-injection traces minus pre-injection traces.

To image the subsurface, the RTM method utilizes the wave fields that are generated by a seismic source and captured by a set of receivers. The measured responses at the receivers consist of direct arrival responses and reflected and/or scattered responses. The traces measured by the receivers are time-reversed and these time-reversed traces are the input waveforms for the receivers acting as sources in a numerical simulation. For example, if the receivers are vertical particle motion geophones, the receivers acting as sources are vertical force sources; if the receivers are pressure receivers, the receivers acting as sources are explosion sources. However, before the traces are time-reversed and played back into the background model, the direct arrivals are generally removed so that only the reflected and/or scattered waves are present in the RTM input waveforms. These time-reversed trace input waveforms applied to the receivers acting as sources produce a time-reversed wave field that propagates into the background model. For the seismic wave propagation, we use a 3D finite-difference electrodynamics algorithm that solves the velocity-stress system of partial differential equations (Aldridge, 2006). A critical part of the RTM process is an imaging condition; *i.e.*, a methodology to produce an image using the time-reversed wave field. One imaging condition is to take the zero-lag cross-correlation between the time-reversed wave field emanating from the receivers acting as sources with the source wave field collapsing onto the source. (Note that one could just as well cross-correlate a collapsing time-reversed wave field with an expanding source wave field.) These two wave fields are like two ships passing in the night and have a maximum in the zero-lag cross-correlation when these two wave fields (two ships) are coincident at the reflection or scattering point in time and hence depth. To apply the RTM process requires a background velocity model for the computation of the time-reversed wave field and the source wave field; therefore, the image is only as good as the background velocity model. Generally, a uniform or smoothly varying model of wave speeds and mass density is used. In order for the image to be independent of the trace length, the zero-lag cross-correlation of the expanding (or collapsing) time-reversed wave field with the collapsing (or expanding) source wave field is the correct procedure.

The RTM method computes numerical solutions to the complete wave equation. This fact makes RTM more attractive in some instances to produce 3D images of the subsurface than Kirchhoff

migration (a workhorse of the petroleum industry), which utilizes a high-frequency ray approximation to the wave equation and therefore has difficulty in multi-path situations (Yoon, *et al*., 2003). RTM is computationally intensive and therefore expensive; in contrast Kirchhoff migration is fast and therefore less expensive. Yoon, *et al*., (2003) showed the advantage of RTM over Kirchhoff for imaging beneath a rugose salt body. For an industry standard model, the SEG/EAGE data set, using a 3D acoustic wave equation, they showed that RTM can image beneath a salt body; whereas Kirchhoff migration fails. Thus, in certain situations, RTM is required to obtain an accurate image of the subsurface.

Figure 3.8 illustrates the time-reversal process. The left-hand panel displays the post-injection traces from vertical geophone receivers along a line $x = 0$ and $-400 \le y \le 400\ m$ for a source at $x = 0,\ y = -400\ m$. The right-hand panel shows the time-reversal of these traces that are the input waveforms to the vertical geophone receivers now acting as vertical body force sources in the numerical process. For each of the 17 sources, there will be 147 receivers acting as sources.

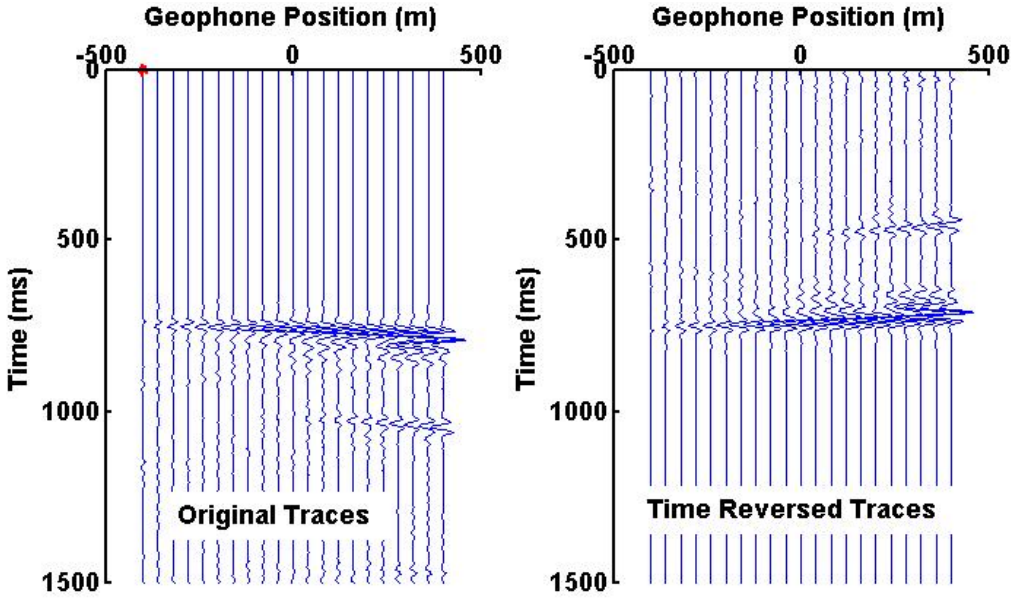

Figure 3.8 Left-hand panel displays the original recorded traces for the source shown as a red dot. The right-hand panel shows the time-reversed traces where now each of the receivers will act as a source in the RTM process.

For the numerical simulation, the time-reversed wave field produced by the receivers acting as sources is captured on a grid of receivers in the subsurface for each of the 17 sources. We now take the zero-lag cross-correlation at each of the grid points of the time-reversed wave field emanating from the receivers acting as sources with the source wave field collapsing onto the source. The image of the subsurface is produced by the maximum in the zero-lag cross-correlation. The 3D RTM images for Model 1 are shown in Figure 3.9, where the left-hand panel is the pre-injection image and the right-hand panel is the post-injection image. These images are plotted on the same color scale. The planes in the images are chosen to intersect at the maximum in the zero-lag cross-correlation. There are some subtle differences in the two images, where the *x*-*z* and *y*-*z* planes are at different positions. Figure 3.10 shows the 2D planar

view of the pre-injection RTM image (left-hand panel) and the post-injection RTM image (right-hand panel). Close inspection shows that there is a difference in these two images. For reference, an outline of the CO_2 target is shown for the post-injection image. For Model 1 with the injection of CO_2, the maximum decrease of V_p is 7.66 percent with a mean decrease of 2.32 percent.

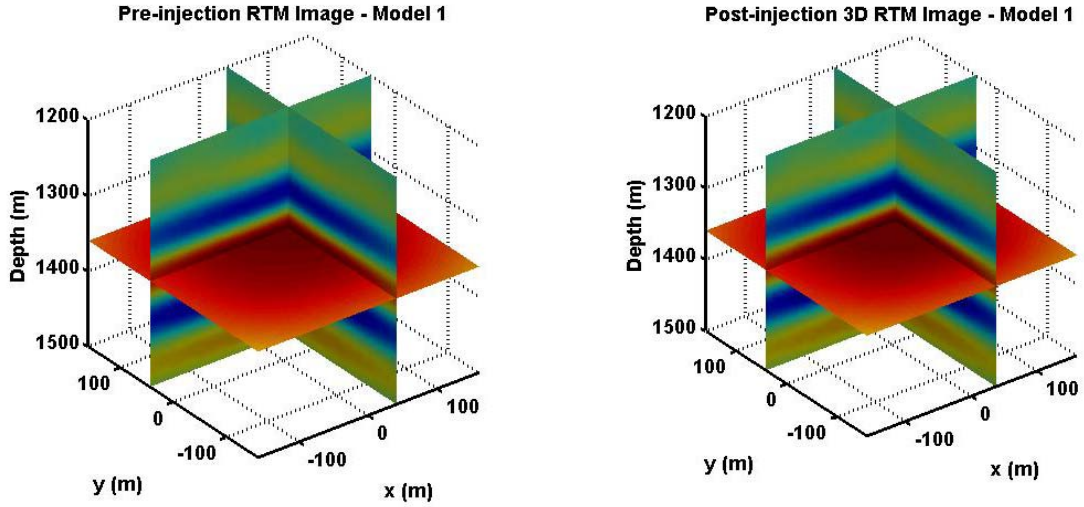

Figure 3.9 3D RTM images pre-injection left-hand panel and post-injection right-hand panel. The two images are plotted on the same color scale. The x-z, y-z, and x-y planes pass through the maximum in the zero-lag cross-correlation.

The image of the CO_2 target is distinct when the pre-injection image is subtracted from the post-injection image. A 3D view is shown in the left-hand panel of Figure 3.11 and a 2D planar view is shown in right-hand panel of Figure 3.11 for Model 1. When the images are differenced, the maximum in the zero-lag cross-correlation image occurs at a depth of 1364 *m*. From an examination of Figure 3.11, the CO_2 affected zone is detected; however the lateral extent is not clear-cut. It should be pointed out that the 25 *Hz* input wavelet results in a wavelength of approximately 160 *m* and one would expect the image to somewhat fuzzy.

At the depth where there is a maximum in the cross-correlation, Figure 3.12 shows the RTM image of the pre-injection state (left-hand panel) and the post-injection state (right-hand panel) for Model 2. As with Model 1, there is a subtle difference between the two images. The outline of the CO_2 affected area is shown for reference. The image of the CO_2 target is distinct when the pre-injection image is subtracted from the post-injection image. A 3D view is shown in the left-hand panel of Figure 3.13 and a 2D planar view is shown in right-hand panel of Figure 3.13 for Model 2. When the images are differenced, the maximum in the zero-lag cross-correlation image occurs at a depth of 1360 *m*. From an examination of Figure 3.13, the CO_2 affected zone is detected; however the lateral extent is not clear-cut. As with Model 1, it should be pointed out that the 25 *Hz* input wavelet results in a wavelength of approximately 160 *m* and one would expect the image to somewhat diffuse. For Model 2 with the injection of CO_2, the maximum

decrease of V_p is 2.67 percent with a mean decrease of 1.57 percent. It is noteworthy that even for the small changes for Model 2, the CO_2 affected zone is detected.

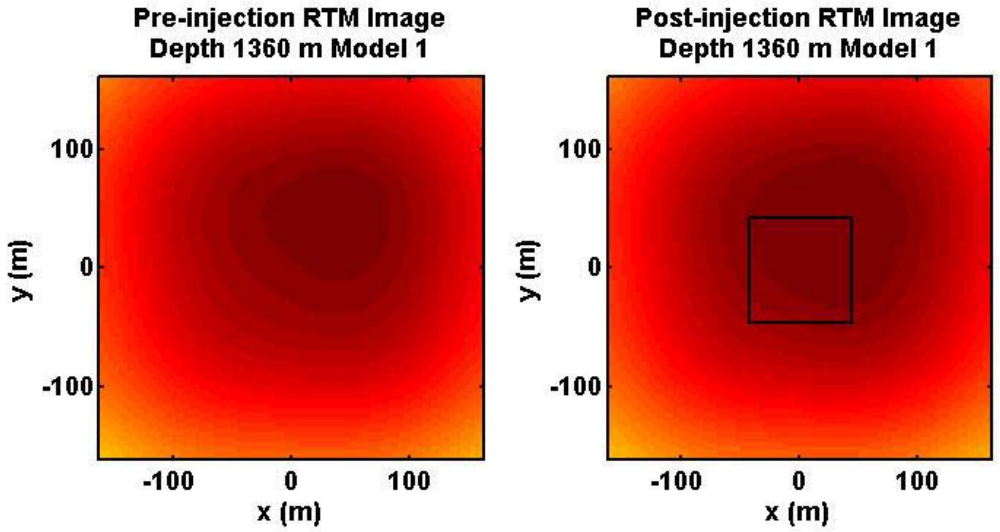

Figure 3.10 Pre-injection (left-hand panel) and Post-injection (right-hand panel) RTM images at a depth of 1360 m for Model 1. The images are plotted with the same color scale. The outline of the CO_2 target is shown for reference.

The field data sets (pre- and post-injection) were analyzed by computing the rms amplitude over a specified time window to capture the energy in the traces corresponding to the P-P reflections. We now examine that method of analysis. Taking the rms amplitude is essentially equivalent to taking the spectral energy over a prescribed time window.

The spectral energy of a trace located at **x** is the zero-lag auto-correlation of the trace depicted here as

$$Spectral\ Energy(\mathbf{x}) = \sum_t f(\mathbf{x},t)^2 = \sum_\omega F(\mathbf{x},\omega)F^*(\mathbf{x},\omega) \tag{3.9}$$

where the * in equation (3.9) represents the complex conjugate. We can determine the spectral energy in a particular time window by segmenting the spectral energy given in equation (3.9).

$$Spectral\ Energy(\mathbf{x},n) = \sum_{t_n}^{t_n+\Delta_n} f(\mathbf{x},t_n)^2 \tag{3.10}$$

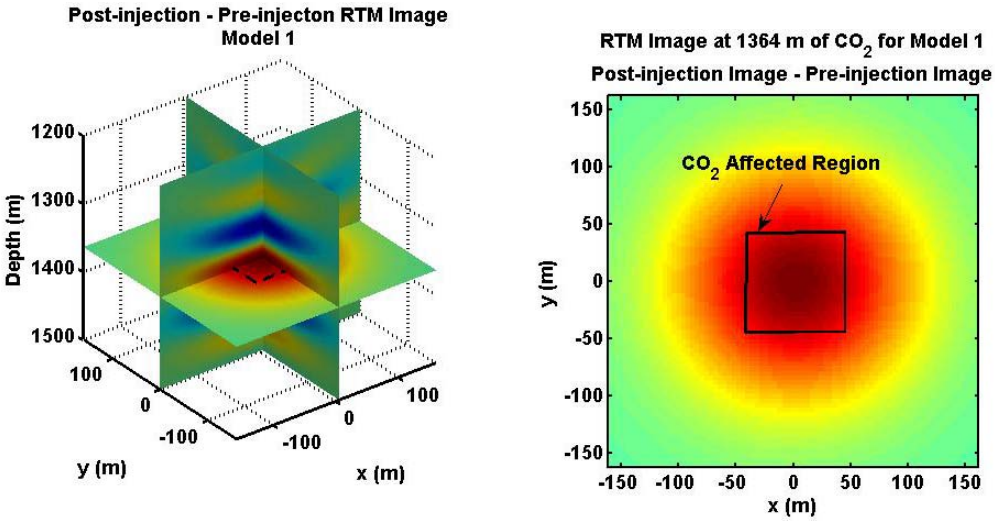

Figure 3.11 Post-injection minus pre-injection RTM images for Model 1. 3D view shown in the left-hand panel and a 2D planar view depth 1364 m is shown in the right-hand panel. An outline of the *CO_2* target is shown for reference.

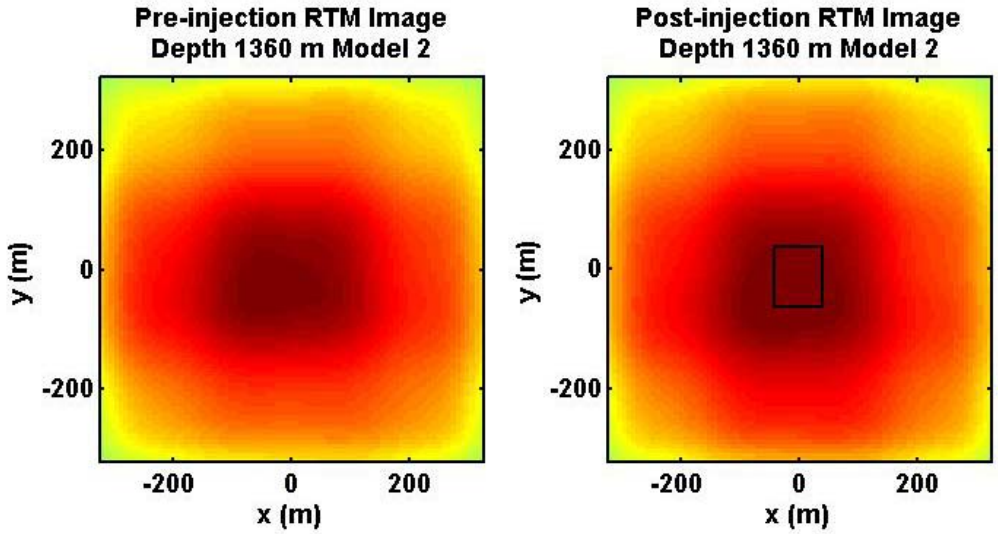

Figure 3.12 Pre-injection (left-hand panel) and Post-injection (right-hand panel) RTM images at a depth of 1360 m for Model 2. The images are plotted with the same color scale. The outline of the *CO_2* target is shown for reference.

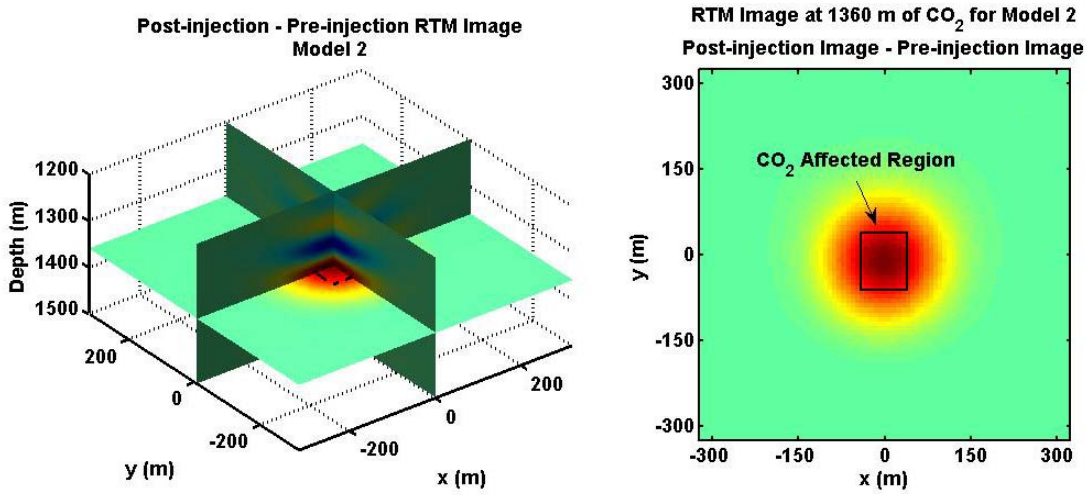

Figure 3.13 Post-injection minus pre-injection RTM images for Model 2. 3D view shown in the left-hand panel and a 2D planar view depth 1360 m is shown in the right-hand panel. An outline of the CO_2 target is shown for reference.

From an examination of the traces in Figure 3.7, most of the spectral energy is in a time window 700-800 *ms*. Figure 3.14, left-hand panel shows the pre-injection spectral energy in the time window 700-800 *ms* summed over all 17 sources for each of the 147 receiver sites for Model 1. The middle panel of Figure 3.14 shows the post-injection spectral energy and the right-hand panel shows the post-injection spectral energy minus the pre-injection spectral energy. Note that the CO_2 target is imaged by neither the post-injection nor the differenced spectral energy. The spectral energy is equivalent to the rms amplitude over a specified time window. These spectral energy plots in Figure 3.14 are based upon the raw trace data where there was no pre-processing except for the removal of the surface waves. The results of this analysis indicates that one should be quite careful in analyzing data using rms amplitudes or spectral energy of the raw data traces as it could easily lead to an erroneous conclusion.

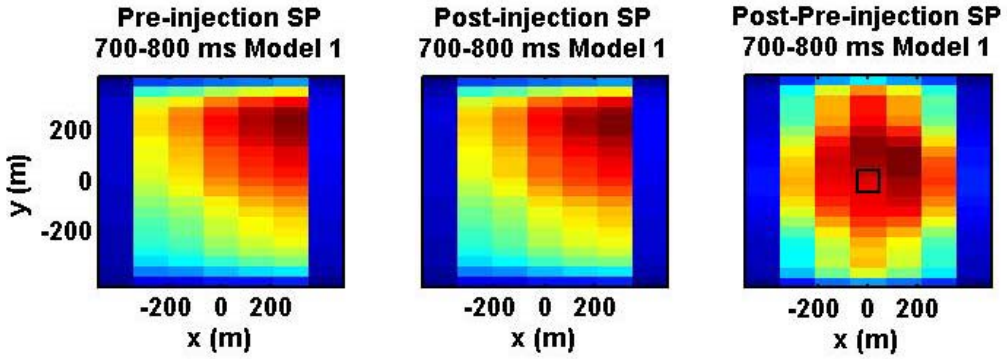

Figure 3.14 Spectral energy over the time window 700-800 ms for Model 1. Pre-injection spectral energy left-hand panel, post-injection spectral energy middle panel, and the differenced spectral energy right-hand panel. Outline of CO_2 target is shown for the differenced spectral energy.

3.7 Numerical Simulation Conclusions

In an attempt to understand the 4D seismic imaging results from the WPQ CO_2 injections experiment, we created two realizations based on the physical parameters of the Shattuck Sandstone storage layer including seismic velocities, densities, porosities, and spatial variability. We then modified the model parameters based on the realistic physical changes in density and bulk module resulting from the CO_2 injection. Seismic waveforms generated through the pre- and post-injection models did show significant variations in amplitudes and differencing the migrated images was able to produce an anomaly correlatable to the injection anomaly, although not highly resolved due to the spatial wavelength of the source used. Simulation of the analysis used for the actual 4D data set on the synthetic data was not as successful in imaging the anomaly and indicated that care must be taken in the processing techniques used to produce images of the post-injection anomalies. This also points out the value in modeling studies to help define and refine analysis techniques and increase the chances of success in the interpretation of expensive field data sets.

It must be noted that, to date, only the vertical component P-wave seismic data from the WPQ seismic imaging experiment have been analyzed. Further exploitation of this data set is recommended to fully understand the changes in seismic response due to the injection and the capability of seismic surveys to image such changes.

4. CONCLUSIONS

The observations on heterogeneities and the measurements of the lateral extents of reservoir-type sandstones in outcrop are compatible with and corroborate the inferences on limited reservoir dimensions made from subsurface data at the West Pearl Queen field. Heterogeneities such as facies changes, local bed thickenings, intraclast conglomerates, channels, and thrust faults interrupt lateral continuity of bedding and would effect the distribution of CO_2. Limited reservoir extents and internal baffles by heterogeneities of the types seen in outcrop may explain the anomalies, such as low CO_2 injection rates, the higher than expected injection pressures, and the observed lag in interwell communication, observed during injection of CO_2 in the West Pearl Queen carbon-dioxide sequestration project. In addition, well-pair correlation data suggest that at least half of the composite sandstone reservoirs have lateral dimensions of less than 1700 to 2500 ft (520 to 760 m), depending on which data set is being used. Permeability drops to less than a millidarcy between reservoirs and at finer-grained sedimentary breaks within reservoirs, limiting vertical continuity within and between reservoirs. Limited reservoir dimensions and internal low-permeability baffles may explain the low CO_2 injection rates, the higher than expected injection pressures, the apparently small seismic anomaly related to CO_2 injection, and the observed lag in interwell communication.

The higher-than-expected injection pressure (which necessitated an injection rate of only 40 tons per day rather than the calculated potential rate of 200 tons per day) and the 3-D seismic results interpreted as a bubble of CO_2 ponded near the injection well, suggest that the individual component beds of the Shattuck reservoir sandstones are not well interconnected, either laterally or vertically, and that even the compound sandstone beds are not laterally extensive. This work analyzed the lateral continuity of the reservoir sandstones utilizing outcrop and subsurface data.

Although the sandstone reservoirs of the Shattuck member occur in distinct zones and although they superficially appear to correlate between wells, they are probably not uniform, vertically-stacked, successive layers of laterally-extensive sandstone, and they are probably not contiguous between wells except at the closest well spacing's. The maximum interpreted lateral extent of the sandy zones along the north-south cross section is 9000 ft (2740 m), but the lateral dimensions of most of these composite reservoirs were probably considerably less, and the larger inferred dimensions may be the result of apparent but spurious correlations.

The methods utilized in this paper to assess the lateral connectivity of reservoir rocks and to capture reservoir heterogeneities are applicable to other geologic sites and could provide a more thorough analysis of a reservoir before CO_2 injection is initiated.

In an attempt to understand the 4D seismic imaging results from the WPQ CO_2 injections experiment, we created two realizations based on the physical parameters of the Shattuck Sandstone storage layer including seismic velocities, densities, porosities, and spatial variability. We then modified the model parameters based on the realistic physical changes in density and bulk module resulting from the CO_2 injection. Seismic waveforms generated through the pre- and post-injection models did show significant variations in amplitudes and differencing the migrated images was able to produce an anomaly correlatable to the injection anomaly, although not highly resolved due to the spatial wavelength of the source used. Part of the analysis of the

field data used the rms amplitude over a specified time window as an indicator of the location of the CO_2 plume. Simulation of that analysis method on the synthetic data was not as successful in imaging the anomaly and indicated that care must be taken in the processing techniques used to produce images of the post-injection anomalies. This also points out the value in modeling studies to help define and refine analysis techniques and increase the chances of success in the interpretation of expensive field data sets.

It must be noted that, to date, only the vertical component P-wave seismic data from the WPQ seismic imaging experiment have been analyzed. Further exploitation of this data set is recommended to fully understand the changes in seismic response due to the injection and the capability of seismic surveys to image such changes.

5. REFERENCES

Aldridge, D. F., 2006, Finite-difference numerical simulation of 3D seismic wave propagation: SAND2006-4302P

Bartel, L. C., Aldridge, D. F., Symons, N. P., and Haney, M. M., 2008, Reverse-time seismic and acoustic wave propagation: high-fidelity subsurface imaging: Sandia National Laboratories Technical Report, SAND2008-0159.

Cooper, S. P., Warpinski, N. R., Pawar, R. J., Stubbs, B. A., Benson, R. D., Grigg, R. B., Svec, R. K., Lorenz, J. C., Bartel, L. C., Krumhansl, J. L., Aldridge, D. F., Holcomb, D. J., Jove-Colon, C. F., Byrer, C., McNemar, A., Westrich, H. R., and Elbring, G. J., 2008, West Pearl Queen CO_2 Sequestration Pilot Test and Modeling Project to 2007: Sandia National Laboratories, Technical Report, in review.

Cooper, S. P., and Lorenz, J. C., 2007, Lateral Extents of Permeability Units: Implications for CO_2 Sequestration at the West Pearl Queen Field, Southeastern New Mexico: Sixth Annual Conference on Carbon Capture and Sequestration, 2007, Pittsburgh, Pennsylvania (not consecutively numbered).

Gassmann, F., 1951, Uber die elastizitat poroser medien: Vierteljahrosschrift der Naturforchenden Gesellschaft in Zurich, **96**, 1-23.

Han, D. and Batzle, M. L., 2004, Gassmann's equation and fluid-saturation effects on seismic velocities: Geophysics, **69**, 398-405.

Hayes, P. T., and Koogle, R. L., 1958, Geology of the Carlsbad Caverns West Quadrangle, New Mexico-Texas: United States Geologic Survey Quadrangle Map GQ 112.

Mazzullo, J., Malicse, A., and Siegel, J., 1991, Facies and depositional environments of the Shattuck Sandstone on the Northwest Shelf of the Permian Basin: Journal of Sedimentary Petrology, vol. **61**, p. 940-958.

Tait, D. B., Ahlen, J. L., Gordon, A., Scott, G. L., Motts, W. S., and Spitler, M. E., 1962, Artesia Group of New Mexico and west Texas: American Association of Petroleum Geologists Bulletin, v. **46**, no. 4, p. 504-517.

Pawar, R.J., Warpinski, N.R., Lorenz, J.C., Benson, R. D., Grigg, R. B., Stubbs, B.A., Stauffer, P.H., Krumhansl, J.P., and Cooper, S.P., 2006, Overview of a CO_2 sequestration field test in the West Pearl Queen reservoir, New Mexico: The American Association of Petroleum Geologists/Division of Environmental Geosciences, Environmental Geosciences, v.**13**, no.3, p.163-180.

Wang, Z., Cates, M. E., and Langan, R. T., 1998. Seismic monitoring of a CO2 flood in a carbonate reservoir: a rock physics study: Geophysics, **63**, 1604-1617.

Yoon, K., Shin, C., Suh, S., Lines, L. R., and Hong, S., 2003, 3D reverse-time migration using the acoustic wave equation: An experience with the SEG/EAGE data set: The Leading Edge, **38**, 38-41.

Yilmaz, O., 1987, Seismic data processing: Society of Exploration Geophysicists.

Distribution

Andrea McNemar
Fuels Resources Division
National Energy Laboratory
Morgantown, WV 26507

Rajesh Pawar
Earth and Environmental Sciences Division
Los Alamos National Laboratories
Los Alamos, NM 87545

Robert D. Benson
Department of Geophysics
Colorado School of Mines
Golden, CO 80401-1887

John C. Lorenz

Sandia National Laboratories

Merson, John A.	06310
Borns, David, J.	06312
Aldridge, David F.	06314
Bartel, Lewis C.	06314
Cooper, Scott P.	06314
Elbring, Gregory J.	06314
Engler, Bruce P.	06314
Symons, Neill P.	06314
Holcomb, David J.	06315
Krumhansl, James L.	06316
Jove-Colon, Carlos F.	06781

Technical Library sanddocs@sandia.gov


Sandia National Laboratories